UNIVERSITY OF ZULULAND

The Effect of Acid Mixtures on Biomass Cellulose Poly (Furfuryl) Alcohol Nanocomposites

By:

Nduduzo Lungisani Khumalo

201860853

BSc. Pure and Applied Chemistry, Honours (UKZN)

THESIS

Submitted to the faculty of Science and Agriculture

In fulfilment of the requirements for the degree

MASTER OF SCIENCE

In the field of

CHEMISTRY

Supervisor: Dr. Samson Mohomane Co-Supervisor: Prof. Tshwafo Motaung

Department of chemistry, University of Zululand

Private Bag X1001, KwaDlangezwa,

3886 South Africa

December 2022

DECLARATION

I hereby declare that the work described in this thesis entitled **"The Effect of Acid Mixtures on Biomass Cellulose Nanocomposites"** is my own work and has not been submitted in any form for another degree or qualification of the University of Zululand or any other University or Institution of tertiary education. Information derived from the published or unpublished work of others has been acknowledged in the text and the list of references is given.

Name: Nduduzo L. Khumalo

Signature…….. Date…….

CERTIFICATION BY SUPERVISORS

This is to certify that this work was carried out by Mr. Nduduzo L. Khumalo in the Department of Chemistry, University of Zululand and is approved for submission in fulfilment of the requirements for the degree of Master of Science in Chemistry.

……

Supervisor

S. Mohomane (PhD)

Doctor of Organic Chemistry

Department of Chemistry, University of Zululand,

KwaDlangezwa, South Africa.

……

Co-Supervisor

T.E. Motaung (PhD)

Professor of Organic Chemistry

Department of Chemistry, University of South Africa,

Florida, South Africa.

DEDICATION

This work is dedicated to my late dad (may his soul rest in peace), my mom, two sisters, brother and my daughter Zanokuhle Khumalo.

ACKNOWLEDGEMENTS

I would like to express my utmost gratitude to my supervisors, Dr. S. Mohomane and Prof. T.E. Motaung for their patience, motivation and immense knowledge. It is through their guidance I have made it this far in this work. I would also like to pass my gratitude for their financial support, without it none of this would be possible.

I would also like to thank University of Zululand (my employer) for offering me a study benefit to pursue my studies.

I am also thankful to my colleagues and the entire staff of the Chemistry Department of University of Zululand and my lab mates; Nthabeleng Hlapisi, Khayelihle Gazu, Thulani Shabangu for their assistance throughout the journey.

Finally, I am most thankful to my family, especially my mother for the emotional support, my brother Sukoluhle, my sisters Gugu and Makhona, Nonjabulo Nkosi for the motivation and encouragement to succeed and my daughter Zanokuhle Khumalo.

TABLE OF CONTENT

DECLARATION ..... **I**
CERTIFICATION BY SUPERVISORS ..... **II**
DEDICATION ..... **III**
ACKNOWLEDGEMENTS ..... **IV**
TABLE OF CONTENT ..... **V**
ABSTRACT ..... **IX**
LIST OF FIGURES ..... **X**
LIST OF TABLES ..... **XII**
LIST OF ABBREVIATIONS ..... **XIII**
LIST OF SYMBOLS AND UNITS ..... **XIV**
CHAPTER 1 ..... **1**
GENERAL INTRODUCTION **1**

1.1. INTRODUCTION 2
1.2. STATEMENT OF THE RESEARCH PROBLEM 4
1.3. SCOPE OF WORK 4
1.4. AIM AND OBJECTIVES 5
1.5. THESIS LAYOUT 5
1.6. REFERENCES 6

CHAPTER 2 ..... **8**
PREPARATION AND ANALYSIS OF CELLULOSE PFA COMPOSITE: CRITICAL REVIEW **9**

2.1. INTRODUCTION 10

2.1.1. Cellulose – the main component of biomass *10*
2.1.2. Poly (furfuryl) alcohol *14*

2.2. CELLULOSE PFA NANOCOMPOSITES 15

2.2.1. Common nanocrystalline cellulose extraction methods *15*
2.2.2. Preparation of cellulose PFA nanocomposites *17*

2.3. THERMAL PROPERTIES 17
2.4. MECHANICAL PROPERTIES 19
2.5. MORPHOLOGICAL CHARACTERISTICS 21
2.6. CONCLUSION 23
2.7. REFERENCES 24

CHAPTER 3 29

THE EFFECT OF H_2SO_4/$HCLO_4$ MIXED ACID CONCENTRATION ON PROPERTIES OF CELLULOSE NANOCRYSTALS FROM SUGARCANE BAGASSE (SCB) 30

3.1. INTRODUCTION 31
3.2. MATERIALS AND METHODS 32

3.2.1. Materials 32
3.2.2. Extraction of cellulose 32
3.2.3. Extraction of cellulose nanocrystals 32

3.3. CHARACTERIZATION METHODS 33

3.3.1. Fourier Transform Infra-Red Spectroscopy 33
3.3.2. X-ray Diffraction 33
3.3.3. Scanning Electron Microscopy 34
3.3.4. Thermogravimetric Analysis 34

3.4. RESULTS AND DISCUSSION 34

3.4.1. FTIR spectroscopy analysis 34
3.4.2. X-ray diffraction analysis 35
3.4.3. Scanning electron microscopy 37
3.4.4. Thermogravimetric analysis 39

3.5. CONCLUSION 41
3.6. REFERENCES 41

CHAPTER 4 45

MORPHOLOGY AND THERMAL PROPERTIES COMPARISON OF GREEN EXTRACTED AND ACETYLATED CNCS FROM MAIZE STALK 46

4.1. INTRODUCTION 47
4.2. MATERIALS AND METHODS 49

4.2.1. Materials 49
4.2.2. Extraction of cellulose 49
4.2.3. Extraction of cellulose nanocrystals (Green Method) 49
4.2.4. Extraction of cellulose nanocrystals 49
4.2.5. Acetylation of cellulose nanocrystals 49

4.3. CHARACTERIZATION METHODS 50

4.3.1. Fourier Transform Infra-Red Spectroscopy 50
4.3.2. X-ray Diffraction 50
4.3.3. Scanning Electron Microscopy 50
4.3.4. Thermogravimetric Analysis 50

4.4. RESULTS AND DISCUSSION 50

4.4.1. FTIR spectroscopy analysis 50
4.4.2. X-ray diffraction analysis 51
4.4.3. SEM analysis 53
4.4.4. TGA analysis 54

4.5. CONCLUSION 56
4.6. REFERENCES 57

CHAPTER 5 61
EFFECT OF ACID HYDROLYSIS ON PROPERTIES OF CELLULOSE/POLY FURFURAL ALCOHOL (PFA) COMPOSITES FROM MAIZE STALK 62

5.1. INTRODUCTION 63
5.2. MATERIALS AND METHODS 64

5.2.1. Materials 64

5.2.2. Extraction of cellulose *64*
5.2.3. Extraction of cellulose nanocrystals *64*
5.2.4. Preparation of cellulose PFA nanocomposites *65*

5.3. CHARACTERIZATION METHODS 65

5.3.1. Fourier Transform Infrared *65*
5.3.2. X-ray Diffraction *65*
5.3.3. Scanning Electron Microscopy *65*
5.3.4. Thermogravimetric Analysis *65*

5.4. RESULTS AND DISCUSSION 66

5.4.1. Fourier transmission infrared *66*
5.4.2. X-ray diffraction analysis *68*
5.4.3. Scanning electron microscope *71*
5.4.4. Thermogravimetric analysis *74*

5.5. CONCLUSION 76
5.6. REFERENCES 76

CHAPTER 6 79

6.1. SUMMARY AND CONCLUSION 80
6.2. RECOMMENDATION 81
6.3. RESEARCH OUTPUTS 82

ABSTRACT

Recently, extraction of cellulose nanocrystals (CNCs) via acid hydrolysis using sulphuric acid has been intensively studied. Moreover, the use of sulphuric acid requires shorter hydrolysis time, while producing stable suspensions with high yield and crystallinity. However, it results in CNCs with lower thermal stability and higher aggregation due to the presence of sulphate ions. Hence, the overall aim of this study is to extract CNCs using mixture of acids and compare its morphology and thermal properties with sulphuric acid hydrolysed CNCs. In addition, the extracted CNCs were encapsulated in a poly (furfural) alcohol (PFA) matrix via in situ polymerization process in the presence of *P*-toluene sulfonic acid as a catalyst to produce cellulose PFA nanocomposites. Furthermore, the study investigates the effect of mixed acid concentration on the morphology, crystallinity and thermal properties. Varying concentrations of 45%, 55% and 65% $H_2SO_4/HClO_4$ hydrolysed CNCs were studied. In conclusion, the study investigated and compared the thermal and morphology of green extracted CNCs and acetylated CNCs. The properties of raw biomass, extracted cellulose, extracted CNCs, and nanocomposites were analysed by Fourier transformed infrared (FTIR), scanning electron microscopy (SEM), X-ray diffraction (XRD) and thermogravimetric analyser (TGA).

H_2SO_4/HNO_4 and H_2SO_4/HCl hydrolysed CNC/PFA nanocomposites showed the highest crystallinity while H_2SO_4/H_3PO4 and $H_2SO_4/HClO_4$ hydrolysed CNC/PFA nanocomposites showed highest thermal stability. The surface breakage and cracked PFA nanocomposite surface observed in SEM was dependent on the strength of acids used to hydrolysed CNCs. $H_2SO_4/HClO_4$ hydrolysed CNC/PFA displayed good dispersion of CNCs in the PFA matrix with no observed surface breakage. With regards to the effect of mixed acid concentration, 55% $H_2SO_4/HClO_4$ hydrolysed CNCs showed the highest crystallinity and thermal stability while 65% $H_2SO_4/HClO_4$ hydrolysed CNCs showed the least thermal stability. SEM results showed fiber breakage for 65% $H_2SO_4/HClO_4$ hydrolysed CNCs which proved to be acid concentration dependent. In conclusion, the acetylated CNCs showed higher crystallinity compared to the green extracted CNCs with evidence of allomorph transformation from cellulose I to cellulose II on the acetylated CNCs. In addition, the acetylated CNCs showed lower thermal stability compared to the green extracted CNCs. SEM also showed a structural transformation upon acetylation of CNCs from a rod like fiber to a crystal-like structure.

List of Figures

Fig. 2.1: Structure of cellulose. 12
Fig 2.2: The chemical structure of a) Furfural (FA) and b) Poly (furfuryl) alcohol (PFA). 14
Figure 2.3: TGA and DTG curves of pure PFA, PFA containing 30, 40 and 50% acid hydrolysed cellulose [33]. 18
Figure 2.4: TGA and DTG curves of MFC (a and b), MFLC (c and d) of composites comprising different amounts of FA [49]. 18
Figure 2.5: DMA results for (a) storage modulus and (b) tan δ curves of pure PFA and cellulose PFA nanocomposites as a function of temperature [33]. 20
Figure 2.6: Fracture surface of PFA nanocomposites incorporating nanocellulose obtained after (a) 30, (b) 40 and (c) 50% acid hydrolysis [34]. 22
Figure 2.7: SEM images of (a) impact fractured surface, (b) tensile fractured surface of PFA/Kenaf 20% [31]. 22
Figure 3.1. FTIR spectra of (a) untreated maize stalk, (b) H_2SO_4 hydrolysed CNC, (c) H_2SO_4/HCl hydrolysed CNC, (d) H_2SO_4/HNO_3 hydrolysed CNC, (e) H_2SO_4/H_3PO_4 hydrolysed CNC and (f) $H_2SO_4/HClO_4$ hydrolysed CNC. 66
Figure 3.3. XRD spectra of (a) untreated maize stalk, (b) H_2SO_4 hydrolysed CNC, (c) H_2SO_4/HCl hydrolysed CNC, (d) H_2SO_4/HNO_3 hydrolysed CNC, (e) H_2SO_4/H_3PO_4 hydrolysed CNC and (f) $H_2SO_4/HClO_4$ hydrolysed CNC. 69
Figure 3.4. XRD spectra of (a) PFA, (b) H_2SO_4 hydrolysed CNC/PFA, (c) H_2SO_4/HCl hydrolysed CNC/PFA, (d) H_2SO_4/HNO_3 hydrolysed CNC/PFA, (e) H_2SO_4/H_3PO_4 hydrolysed CNC/PFA and (f) $H_2SO_4/HClO_4$ hydrolysed CNC/PFA. 71
Figure 3.5. SEM images of (a) untreated maize stalk, (b) H_2SO_4 hydrolysed CNC, (c) H_2SO_4/HCl hydrolysed CNC, (d) H_2SO_4/HNO_3 hydrolysed CNC, (e) H_2SO_4/H_3PO_4 hydrolysed CNC and (f) $H_2SO_4/HClO_4$ hydrolysed CNC. 72
Figure 3.6. SEM images of (a) PFA, (b) H_2SO_4 hydrolysed CNC/PFA, (c) H_2SO_4/HCl hydrolysed CNC/PFA, (d) H_2SO_4/HNO_3 hydrolysed CNC/PFA, (e) H_2SO_4/H_3PO_4 hydrolysed CNC/PFA and (f) $H_2SO_4/HClO_4$ hydrolysed CNC/PFA. 73
Figure 3.7. TGA(A) and DTG(B) of (a) untreated maize stalk, (b) H_2SO_4 hydrolysed CNC, (c) H_2SO_4/HCl hydrolysed CNC, (d) H_2SO_4/HNO_3 hydrolysed CNC, (e) H_2SO_4/H_3PO_4 hydrolysed CNC and (f) $H_2SO_4/HClO_4$ hydrolysed CNC. 74

Figure 4.1: FTIR spectra of the raw sugarcane bagasse, cellulose, 45% H_2SO_4 hydrolysed CNCs, 45% H_2SO_4/$HClO_4$ hydrolysed CNCs, 55% H_2SO_4/$HClO_4$ hydrolysed CNCs and 65% H_2SO_4/$HClO_4$ hydrolysed CNCs..... 35
Figure 4.2: XRD spectra of the raw sugarcane bagasse, cellulose, 45% H_2SO_4 hydrolysed CNCs, 45% H_2SO_4/$HClO_4$ hydrolysed CNCs, 55% H_2SO_4/$HClO_4$ hydrolysed CNCs and 65% H_2SO_4/$HClO_4$ hydrolysed CNCs..... 37
Figure 4.3: SEM images of the (a) the raw sugarcane bagasse, (b) cellulose, (c) 45% H_2SO_4 hydrolysed CNCs, (d) 45% H_2SO_4/$HClO_4$ hydrolysed CNCs, (e) 55% H_2SO_4/$HClO_4$ hydrolysed CNCs and (f) 65% H_2SO_4/$HClO_4$ hydrolysed CNCs. 38
Figure 4.4: TGA curve of the raw sugarcane bagasse, cellulose, 45% H_2SO_4 hydrolysed CNCs, 45% H_2SO_4/$HClO_4$ hydrolysed CNCs, 55% H_2SO_4/$HClO_4$ hydrolysed CNCs and 65% H_2SO_4/$HClO_4$ hydrolysed CNCs..... 39
Figure 4.5: DTG curve of the raw sugarcane bagasse, cellulose, 45% H_2SO_4 hydrolysed CNCs, 45% H_2SO_4/$HClO_4$ hydrolysed CNCs, 55% H_2SO_4/$HClO_4$ hydrolysed CNCs and 65% H_2SO_4/$HClO_4$ hydrolysed CNCs..... 40
Figure 5.1: FTIR spectra of the raw maize stalk, extracted cellulose, green extracted CNCs, and acetylated CNCs. 51
Figure 5.2: XRD spectra of the raw maize stalk, extracted cellulose, green extracted CNCs, and acetylated CNCs. 52
Figure 5.3: SEM images of (a) raw maize stalk, (b) extracted cellulose, (c) green extracted CNCs, and (d) acetylated CNCs..... 54
Figure 5.4: FTIR spectra of the raw maize stalk, extracted cellulose, green extracted CNCs, and acetylated CNCs. 55
Figure 5.5: DTG spectra of the raw maize stalk, extracted cellulose, green extracted CNCs, and acetylated CNCs. 56

LIST OF TABLES

Table 2.1: Lignin and cellulose contents in several types of biomasses 12

Table 2.2: Mechanical properties of various materials 13

Table 2.3: Mechanical properties of different types of cellulose 13

Table 3.1. Crystalline Index values of materials studied using Segal and deconvolution methods 68

Table 3.2. Crystalline Index values of cellulose (PFA) nanocomposites studied using deconvolution methods. 70

Table 4.1. Crystalline Index values of materials studied using Segal and deconvolution methods. 36

Table 5.1. Crystalline Index values of materials studied using Segal and deconvolution methods 53

LIST OF ABBREVIATIONS

PFA	Poly (furfural) alcohol
FA	Furfural alcohol
CNCs	Cellulose nanocrystals
PVC	Polyvinyl chloride
CSIR	Council for scientific and industrial research
PPC	Portland pozzolana cement
OPC	Ordinary Portland cement
Fig	Figure
DP	Degree of polymerisation
XRD	X-ray diffraction
NCC	Nanocrystalline cellulose
DTG	Differential thermogravimetric
TGA	Thermogravimetric analyser
MFC	Microfibrillated cellulose
MFLC	Microfibrillated lignocellulose
DMA	Dynamic mechanical analyser
Tg	Transition temperature
SEM	Scanning electron microscopy
TEM	Transmission electron microscopy
CPS	Chemically purified cellulose
FTIR	Fourier transform infrared spectroscopy
ATR	Attenuated total reflection
CI	Crystallinity index
NaOH	Sodium Hydroxide
NaOCl	Sodium hypochlorite
H_2SO_4	Sulphuric acid
HNO_3	Nitric acid
$H3PO_4$	Orthophosphoric acid
$HClO_4$	Perchloric acid
OH	Hydroxyl
H_2S	Hydrogen sulphide

LIST OF SYMBOLS AND UNITS

Ppmv	parts per million by volume
Wt	weight
MPa	Mega pascal
Cm	Centimetre
g	grams
min	minutes
s	seconds
phr	parts per hundred rubbers
%	Percentage
δ	delta
θ	theta
σ	sigma
Σ	sum
μ	micro
°C	degrees Celsius
mg	milligram
ml	millilitre
KV	kilovolts

CHAPTER 1

GENERAL INTRODUCTION

1.1. Introduction

Cellulose is the most abundant biopolymer and organic compound on earth. Due to the growing need for environmentally friendly polymer composites, several researchers have investigated ways to transform by-products into valuable eco-friendly polymer composites. South Africa is one of Africa's most productive agricultural countries. Sugarcane, maize, and timber cropping are among the most important agricultural operations. Burning is the most common method of disposal, which results in air pollution as well as an increased carbon footprint, which contributes to global warming. The use of this biomass (waste) to produce polymer nanocomposites could help to reduce carbon emissions and provide a more sustainable plastic polymer manufacturing process. Cellulose has been derived from plants, animals (tunicates), algae, and bacteria, among other sources. Nanocrystalline cellulose has shown basic "building blocks" with features properties like homogeneity and endurance, which are important for the second generation of cellulose-based products and engineering applications.

The use of renewable materials has been driven by economic and environmental concerns for the advancement of economically responsive materials. Most researchers are increasingly focusing on these types of materials. Furfural alcohol (FA) is a good starting material for making a variety of monomers. It has the benefit of being economically obtained by hydrolysis of forestry and agricultural waste that contain significant levels of pentoses. [1-4]. Biomass, such as sugarcane bagasse and corncobs, can be used to make furfural. Furfuryl alcohol is made via a simple reduction of furfural. As a result, FA is a green chemical that is both renewable and cost-effective. Polymerization of FA leads to the formation of Poly (furfuryl alcohol) (PFA). PFA is a cross-linked thermosetting polymer that is usually made by polymerizing FA with a mineral, organic, or Lewis acid catalyst. [5-9]. FA polymerization catalysed by acid produces a black cross-linked product. The mechanism of crosslinking and colouration has been investigated in depth. The hydrogen atoms in the methylene connections between the two furan rings appear to be highly important in favouring the side reactions related with chain crosslinking and colour creation. [1-7]. Moulds, corrosion-resistant coatings, polymer concrete, metal-casting cores, sand consolidation and well plugging, wood adhesives and binders, modifier for natural fibre surfaces, low flammability, low smoke release, possessing of materials, and precursor for

carbon nanocomposites and glassy carbons are just a few of the many applications for PFA. [3, 10, 11]. In some applications in literature, cellulose has been used as fillers in the preparation of composite materials [12, 13]. In addition, due to environmental compatibility and economic reasons, recent studies are interested in the PFA composites containing cellulose as fillers [14-17].

There are several advantages associated with the usage of cellulose as the main materials in several applications, cellulose is:

- An abundant compound worldwide, there are a wide variety of fibres available worldwide.
- Biodegradable in the environment and carbon dioxide neutral.
- Fairly cheap and easy to obtain.
- Sustainable.
- Renewable.
- High biocompatibility and
- Formed using solar energy.

Cellulose has other structural advantages which make it a useful raw material, cellulose has:

- High modulus and specific strength, 128 GPa is the supreme macroscopic plant cellulose fibre Young's modulus [18];
- A comparatively reactive surface, that proves useful when modifying the surface.
- High sound damping performance as a result in fibres which are structurally hollow and
- Lower density.

Composites reinforced with natural fibres has a shortage of industrial applications due because of the following shortcomings:

- Due to polarity and hydrophilic nature of cellulose fibres, these composites are non-compatible with hydrophobic and non-polar thermoplastics, this

consequence in a fragile interaction between the reinforcement and the matrix as well as the ineffective distribution of the reinforcement.

- Cellulose fibres compounding is restricted by the processing temperature with chief engineering plastics for instance polypropylene, poly (vinyl chloride), polyethylene as well as polystyrene.
- These composites swell leading to the decrease in properties such as mechanical and they can be hydroscopic.

1.2. Statement of the research problem

Cellulose is one of the most plentiful biopolymer and organic compound on planet earth. The use of traditional chemicals to produce plastic polymers has accelerated all kinds of pollution as well as global warming concerns. Cellulose nanocomposites have been viewed as the potential solution due to their sustainable and renewable properties. In this study, furfural has been chosen as a suitable starting material as it can be obtained from hydrolysis of forestry and agricultural waste. It is also obtained from biomass such as sugarcane bagasse, corncobs etc. Therefore, FA is regarded as a green chemical that is both renewable and economical. Few researchers have studied cellulose PFA nanocomposites, and the results have been promising when it comes to thermal stability and mechanical strength which are basic properties of plastic polymers. It has been proven that sulphuric acid provides best properties of nanocrystalline cellulose however, none has investigated the effect of mixture of acids on different biomass to produce cellulose PFA nanocomposites. This greener approach to produce plastic polymers with improved chemical properties will have a positive effect on cost, human health, eco-friendly, biocompatibility and the environment.

1.3. Scope of work

The work has been divided into three parts; the first part is the extraction of cellulose from maize stalk and sugarcane bagasse. The second part of the study is the extraction of cellulose nanocrystals via acid hydrolysis. This study focusses more on the use of acid mixtures to extract cellulose nanocrystals which is also the novelty of this study.

Furthermore, the cellulose nanocrystals are encapsulated in a PFA matrix to produce a plastic material.

1.4. Aim and Objectives

The aim of the study is to investigate the effect of acid mixtures on biomass cellulose PFA nanocomposites. The above-mentioned broad aim is below broken down to several objectives that also represent the milestones needed to be achieved to realize the aim. The objectives are:

- To extract cellulose from sugarcane bagasse and maize stalk.
- To extract cellulose nanocrystals from the extracted cellulose using mixture of acids.
- To reinforce PFA with cellulose nanocrystals using in-situ polymerization process.
- To investigate the effect of acid hydrolyses on properties of cellulose/PFA composites from maize stalk.
- To investigate the effect of H_2SO_4/$HClO_4$ mixed acid concentration on properties of cellulose nanocrystals from sugarcane bagasse (SCB).
- To investigate the morphology and thermal properties of green extracted and acetylated CNCs from maize stalk.

1.5. Thesis Layout

The thesis is composed of 6 chapters which are briefly described below

1. **Chapter 1**: General introduction.
2. **Chapter 2**: Synthesis of cellulose PFA nanocomposite, A critical review.
3. **Chapter 3**: The effect of H_2SO_4/$HClO_4$ mixed acid concentration on properties of cellulose nanocrystals from sugarcane bagasse (SCB).
4. **Chapter 4**: Morphology and thermal properties comparison of green extracted and acetylated CNCs from maize stalk.
5. **Chapter 5**: Effect of Acid Hydrolyses on Properties of Cellulose/Poly Furfural Alcohol (PFA) Composites from Maize Stalk.
6. **Chapter 6**: Conclusion, summary of the overall work and future recommendations.

1.6. References

1. Gandini, A., *Furans as offspring of sugars and polysaccharides and progenitors of a family of remarkable polymers: a review of recent progress.* Polymer Chemistry, 2010. **1**(3): p. 245-251.
2. Belgacem, M.N. and A. Gandini, *Materials from vegetable oils: major sources, properties and applications*, in *Monomers, polymers and composites from renewable resources*. 2008, Elsevier. p. 39-66.
3. Gandini, A. and M.N. Belgacem, *Furans in polymer chemistry.* Progress in Polymer Science, 1997. **22**(6): p. 1203-1379.
4. Moreau, C., M.N. Belgacem, and A. Gandini, *Recent catalytic advances in the chemistry of substituted furans from carbohydrates and in the ensuing polymers.* Topics in Catalysis, 2004. **27**(1-4): p. 11-30.
5. Choura, M., N.M. Belgacem, and A. Gandini, *Acid-catalyzed polycondensation of furfuryl alcohol: Mechanisms of chromophore formation and cross-linking.* Macromolecules, 1996. **29**(11): p. 3839-3850.
6. Principe, M., P. Ortiz, and R. Martínez, *An NMR study of poly (furfuryl alcohol) prepared with p-toluenesulphonic acid.* Polymer international, 1999. **48**(8): p. 637-641.
7. González, R., J.M. Figueroa, and H. González, *Furfuryl alcohol polymerisation by iodine in methylene chloride.* European Polymer Journal, 2002. **38**(2): p. 287-297.
8. Song, C., T. Wang, and J. Qiu, *Preparation of C/CMS composite membranes derived from Poly (furfuryl alcohol) polymerized by iodine catalyst.* Desalination, 2009. **249**(2): p. 486-489.
9. Cesano, F., et al., *Synthesis of ZnO–carbon composites and imprinted carbon by the pyrolysis of ZnCl2-catalyzed furfuryl alcohol polymers.* Journal of Photochemistry and Photobiology A: Chemistry, 2008. **196**(2-3): p. 143-153.
10. Wang, H. and J. Yao, *Use of poly (furfuryl alcohol) in the fabrication of nanostructured carbons and nanocomposites.* Industrial & engineering chemistry research, 2006. **45**(19): p. 6393-6404.
11. Trindade, W.G., et al., *Phenolic thermoset matrix reinforced with sugar cane bagasse fibres: attempt to develop a new fibre surface chemical modification involving formation of quinones followed by reaction with furfuryl alcohol.* Macromolecular Materials and Engineering, 2004. **289**(8): p. 728-736.
12. Roghani-Mamaqani, H., et al., *Furfuryl alcohol functionalized graphene nanosheets for synthesis of high carbon yield novolak composites.* Journal of Applied Polymer Science, 2014. **131**(11).

13. Deka, H., M. Misra, and A. Mohanty, *Renewable resource based "all green composites" from kenaf biofibre and poly (furfuryl alcohol) bioresin.* Industrial Crops and Products, 2013. **41**: p. 94-101.
14. Ahmad, E., A. Luyt, and V. Djoković, *Thermal and dynamic mechanical properties of bio-based poly (furfuryl alcohol)/sisal whiskers nanocomposites.* Polymer bulletin, 2013. **70**(4): p. 1265-1276.
15. Motaung, T., et al., *The effect of acid content on the poly (furfuryl) alcohol/cellulose composites.* Polymer Composites, 2016. **37**(8): p. 2434-2441.
16. Motaung, T.E., et al., *Agave and sisal fibre-reinforced polyfurfuryl alcohol composites.* Journal of Thermoplastic Composite Materials, 2017. **30**(10): p. 1323-1343.
17. Pranger, L.A., G.A. Nunnery, and R. Tannenbaum, *Mechanism of the nanoparticle-catalyzed polymerization of furfuryl alcohol and the thermal and mechanical properties of the resulting nanocomposites.* Composites Part B: Engineering, 2012. **43**(3): p. 1139-1146.
18. Page, D., F. El-Hosseiny, and K. Winkler, *Behaviour of single wood fibres under axial tensile strain.* Nature, 1971. **229**(5282): p. 252.
19. Chazeau, L., et al., *Viscoelastic properties of plasticized PVC reinforced with cellulose whiskers.* Journal of Applied Polymer Science, 1999. **71**(11): p. 1797-1808.
20. Dufresne, A., M.B. Kellerhals, and B. Witholt, *Transcrystallization in Mcl-PHAs/cellulose whiskers composites.* Macromolecules, 1999. **32**(22): p. 7396-7401.
21. Luo, J.-J. and I.M. Daniel, *Characterization and modeling of mechanical behavior of polymer/clay nanocomposites.* Composites science and technology, 2003. **63**(11): p. 1607-1616.
22. Terech, P., L. Chazeau, and J. Cavaille, *A small-angle scattering study of cellulose whiskers in aqueous suspensions.* Macromolecules, 1999. **32**(6): p. 1872-1875.
23. Alexandre, M. and P. Dubois, *Polymer-layered silicate nanocomposites: preparation, properties and uses of a new class of materials.* Materials Science and Engineering: R: Reports, 2000. **28**(1-2): p. 1-63.
24. Dubief, D., E. Samain, and A. Dufresne, *Polysaccharide microcrystals reinforced amorphous poly (β-hydroxyoctanoate) nanocomposite materials.* Macromolecules, 1999. **32**(18): p. 5765-5771.

CHAPTER 2

PREPARATION AND ANALYSIS OF CELLULOSE PFA COMPOSITE: CRITICAL REVIEW

Published in:
Cellulose Chemistry and Technology. 55, 299-309.
https://doi.org/10.35812/CelluloseChemTechnol.2021.55.30

2.1. Introduction

Because of the depletion of fossil fuels and the generation of large quantities of harmful wastes, in recent years, there has been a huge interest worldwide in sustainable production due to the depletion of raw materials, generation and safe disposal of large quantities of harmful waste. The use of biomass is one way of ensuring sustainable production of chemicals and other value-added materials. Hence, researchers are constantly looking for better methods of incorporating biomass in production of chemicals and other materials, such as composites. Moreover, there is a huge interest in finding alternatives to replace traditional methods of developing both chemicals and plastics. Biocompatible composites and biodegradable plastics made from biomass has been promising solution to replace petrochemical based polymers, to diminish the universal dependence on fossil fuel sources and achieve a simplified end-of-life disposal. In the literature, biomass is often referred to as lignocellulose material [19].

2.1.1. Cellulose – the main component of biomass

Lignocellulose materials are composed of their constituent of biopolymers, which are lignin, cellulose and hemicellulose. The content of lignin and cellulose in lignocellulose biomass differs among species as shown in Table 2.1. Lignin content evaluation in the biomass is important from a technological point of view to optimize the mechanical and chemical pre-treatment parameters necessary to produce pure cellulose pulp [19]. Cellulose (see Figure 2.1) is the most common organic compound and most abundant biopolymer on earth and comprises about 33 percent of all plant matter. The amount of cellulose produced each year is about $1{,}5 \times 10^{12}$ tons [20]. Therefore, it remains one of the readily available raw materials in nature. Cellulose fibres have been widely studied for their application in eco-friendly composite material, but their full application potentials have not been completely exhausted [9-15].

The presence of several hydroxyl (OH) groups in cellulose is responsible for multiple hydrogen bonds, which are formed between the oxygen and the hydrogen molecules. These intra- and intermolecular bonds are responsible for the high tensile strength of cellulose microfibrils, which comprise crystalline, paracrystalline and amorphous regions [8].

Theoretically, the elastic modulus and tensile strength are 150 and 10 GPA, respectively, for a perfect cellulose structure [9]. The degree of polymerisation (DP) ranges from 300 in wood fibres up to 10,000 for bacterial and plant fibres [2]. Interestingly, the DP, cellulose content and the lateral arrangement of microfibrils exert the principal influence on the tensile properties of a plant fibre.

Over the years, cellulose has been widely used in the form of fibre and as an energy source. The use of natural cellulose is even more extensive nowadays, hence, the ever-increasing textile, forest and paper industries. These uses have been termed by a few authors as *first-generation* uses of cellulose [10]. Another important field of cellulose application is in engineering polymer systems, as reinforcement in composite materials [6]. However, cellulose has some weaknesses, such as its incompatibility with the hydrophobic polymer matrix, the tendency to form aggregates during processing and the water-swellable nature of cellulose, particularly in its amorphous regions [11]. These drawbacks greatly reduce the potential of natural fibres to be utilised as reinforcements in polymers. In addition, there are other factors that greatly influence the properties of cellulose, including the harvesting period, the type of plant and the part of the plant from which is it extracted [12].

Uniformity and durability are new properties necessary for the second generation of cellulose-based products and their engineering applications. These properties can be imparted by the elementary building blocks of cellulose, known as nanocrystalline cellulose (NCC) [1]. NCC is the basic reinforcement unit, which strengthens all consequent structures in trees and plants. NCC contains only a small number of defects, meaning its axial Young's modulus is extraordinary, and close to the one derived from theoretical chemistry. It is hypothetically stronger than Kevlar, and within the range of other reinforcement materials (Table 2.1) [1]. This property makes NCC a useful material that can be applied as filler in polymer composite engineering. As may be noted in Table 2.1, the experimental strength of NCC is very high, while it has low density, high aspect ratio and high surface area. It also possesses modifiable surface properties due to the presence of reactive hydroxyl side groups. Furthermore, cellulose nanoparticles have been found to biodegrade in an aqueous environment more rapidly than other commonly used nanoparticles, such as carbon nanotubes [1].

Table 2.1: Lignin and cellulose contents in several types of biomasses

Type of biomass	Lignin (wt.%)	Cellulose (wt.%)	References
Wood	10-35	40-60	[21]
Sun	6	80	[22]
Ramie	1	76	[22]
Corn cob	20	70	[23]
Flax fibres	2-3	60-81	[23]
Coir fibres	45	43	[24]
Sugarcane bagasse	20	40	[24]
Wheat straw	15	30	[22]
Sisal fibres	4-12	43-88	[24]
Corn stover	14	33	[23]
Cotton stalk	18	65	[23]
Hemp fibres	3.7-5	70-78	[24]
Rice-husk	35	55	[23]
Rice-straw	18	62	[23]
Pineapple leaf fibres	3-4	79-83	[25]
Pine-sawdust	30	60	[23]
Kenaf fibres	18	36	[24]

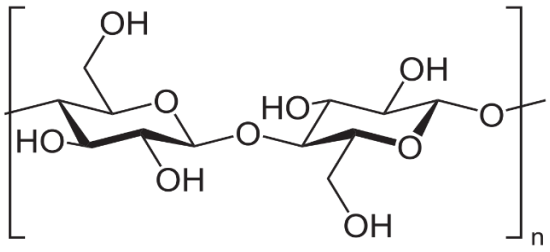

Fig. 2.1: Structure of cellulose.

Table 2.2: Mechanical properties of various materials

Materials	**σ (MPa)**	**E (GPa)**	**Density (g/cm^3)**	**References**
Crystalline cellulose	7500-7700	110-220	1.6	[26]
Aluminium	330	71	2.7	[19]
Stainless steel	1280	210	7.8	[27]
Softwood kraft pulp	700	20	1.5	[27]
Kevlar fibre	3880	88	1.4	[28]

The mechanical properties of different types of cellulose (Table 2.3) reveal variation in terms of tensile strength, cellulose I exhibit the highest tensile strength and cellulose III_2 – the least tensile strength. This variation is caused by the dissimilarity in the molecular structure of different cellulose allomorphs. Changes in molecular structure are caused by deformation mechanisms, involving complex stretching and re-organization of the hydrogen bonds. This varies significantly for crystalline and amorphous phases. The mechanical properties of cellulose are comparable with those of other engineering materials, such as aluminium (70 GPa) and glass fibres (76 GPa) [15] Due to the low density (1.581.59 g/cm^3) of native cellulose,

Table 2.3: Mechanical properties of different types of cellulose

Type of cellulose	**Young's Modulus (GPA)**	**Technique used**	**Reference**
Amorphous cellulose	10.3	Force field model	[29]
Cellulose fibril of ramie fibre	134	XRD	[30]
Cellulose I	138	XRD	[31]
Cellulose II	88	XRD	[31]
Cellulose III_1	87	XRD	[31]
Cellulose III_2	58	XRD	[31]
Cellulose IV	75	XRD	[31]

Wegst et al. [17] ranked its specific stiffness of 67 GPa amongst the highest of all natural materials [16]. Cellulose I is considered as the strongest allomorph, with a theoretical definitive tensile strength between 13-17 GPa. The low density and high tensile strength of the native cellulose crystal results is the highest specific tensile strength of any known natural polymers for cellulose I (667 MPa cm3 g-1) [2].

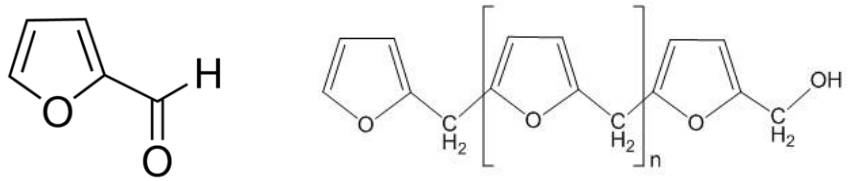

a) FA **b) PFA**

Fig 2.2: The chemical structure of a) Furfural (FA) and b) Poly (furfuryl) alcohol (PFA).

2.1.2. Poly (furfuryl) alcohol

The environmental and economic concerns for the development of eco-friendly materials have led to the exploitation of renewable resources. Furfural is a suitable starting material for the synthesis of several monomers. It presents several advantages, as it can be economically obtained from the hydrolysis of forestry and agricultural wastes, which contain pentose in sufficient amounts [19-22]. Furfural can be obtained from biomass, such as sugarcane bagasse, corncobs etc. A simple reduction process of furfural prepares furfuryl alcohol (FA). Thus, FA can be considered as a green chemical, which is both renewable and economical. Poly (furfural alcohol) (PFA) is a cross-linked thermosetting polymer that is normally produced via a mineral, organic or Lewis acid-catalysed polymerization of FA (see Fig. 2.2) [23-27]. Acid catalysed polymerization of FA results in a dark cross-linked product. Studies have been carried out to understand the mechanism of coloration and crosslinking. Apparently, hydrogen atoms of the methylene bridges between two furan rings play a crucial part in favouring the side reactions associated to colour formation and crosslinking of chains [19-25]. PFA is widely applied in different fields, including metal-casting cores, polymer composites, corrosion resistant coatings, sand consolidation, wood adhesives and binders. It has also been used as precursor for glassy carbons and carbon nanocomposites, as modifier for natural fibre surfaces, and a component to achieve materials with low flammability and low smoke release [21,28,29].

Thus, there has been intense research interest in developing PFA composites containing cellulose [30-35].

2.2. Cellulose PFA nanocomposites

A cellulose PFA nanocomposite refers to cellulose used as a filler dispersed in a PFA matrix. The PFA matrix is typically produced from biomass waste and is like a phenolic resin, but without the toxicity of phenol and formaldehyde compounds. PFA is generally used in applications requiring flame retardancy, high char yield and low smoke release [35]. Recent studies showed that cellulose at nanoscale provides a significantly higher surface area than most traditional fillers, often leading to improved thermal and mechanical properties when incorporated in a PFA matrix [36-39]. Several methods have been used to extract NCC for reinforcing PFA nanocomposites, including sulphuric acid hydrolysis. Sometimes, certain issues, such as matrix-filler interaction, pose significant processing challenges in the development of cellulose PFA nanocomposites. The high viscosity and van der Waals attraction between filler particles also provide a challenge in the production of uniform, stable dispersions of the nanoparticles throughout the matrix [40]. To overcome these issues and achieve the desired filler dispersion in the polymer matrix, optimization of the filler content and a controlled environment are often required [36,41]. The following section summarizes cellulose extraction methods reported in the literature for further development of PFA nanocomposites, the preparation routes of cellulose PFA composites, as well as the mechanical, thermal and morphological characteristics of the achieved materials, according to recent literature sources.

2.2.1. Common nanocrystalline cellulose extraction methods

The extraction or isolation of NCC from the cellulose source material generally involves two steps. The first is the pre-treatment of the raw material. For example, for wood and plants, it includes the complete or partial removal of the matrix components, such as lignin, hemicelluloses and pectin. The second step consists in the chemical treatment of the isolated cellulosic fibres; usually acid hydrolysis is performed to remove the amorphous regions of the cellulose polymer. The pre-treatment step is similar for plants and wood source materials. The same technique as the one used in the pulp and paper industry is applied here. Lignin hinders the isolation of cellulosic fibres from the source material; therefore, its removal is essential in

obtaining NCC. In general, the process involves grinding the source material to depolymerize the lignin and hemicelluloses. It is followed by chemical treatment of biomass to solubilize lignin and hemicelluloses, and subsequent bleaching with oxidizing agents, such as hypochlorite, potassium permanganate and potassium dichromate.

There is another alternative pre-treatment process known as steam explosion, which has attracted much research interest in the past two decades. The method is primarily inexpensive, and allows converting lignocellulose material into nanocellulose [7,42,43]. During this process, the lignocellulose material in the digester is firstly pulverized and exposed to high-pressure steam for a short time (usually, 20 s to 20 min) at a pressure of about 14-16 bar and temperature of 200-270 °C. The pressure in the digester is then dropped by releasing the steam and exposing the sample to normal atmospheric pressure. This results in explosion, which breaks down the lignocellulose structure, thus removing most of the water-soluble fraction of hemicelluloses and the lower molecular weight fraction of lignin. However, some of the lignin that remains might require mercerization for complete extraction. If the optimal conditions are met, the above process allows for complete removal of lignin and hemicelluloses, while leaving cellulose moieties intact [3].

The most widely used method of extracting NCC from cellulose remains controlled sulphuric acid hydrolysis due to the stability of the resulting suspensions [44-47]. The general procedures for the extraction of NCC consist of the following steps:

The cellulosic material is hydrolysed using a strong acid under strictly controlled conditions of time, temperature, agitation, and with control of other conditions, such as concentration and nature of the acid and the acid to cellulose ratio.

Dilution with distilled water to quench the reaction and repeated washing with successive centrifugation.

Comprehensive dialysis against distilled water to fully eliminate free acid molecules.

Mechanical treatment, commonly sonication, to separate the nanocrystals as a constant stable suspension.

Subsequent concentration and freeze-drying of the suspension to produce solid NCC.

2.2.2. Preparation of cellulose PFA nanocomposites

Various preparation methods have been reported in the literature for developing cellulose PFA nanocomposites. Pranger and co-workers [35] dispersed 0.75 phr freeze-dried cellulose nanocrystals in FA by means of an ultra-sonication treatment. This was followed by heating the reaction mixture until the formation of the resin. Similarly, Ahmad et al. [32] also added freeze-dried nanocrystals to FA and subjected the mixture to sonication. However, after the sonication treatment, a monohydrate was added to catalyse the polymerization process. The resulting mixture was heated until the formation of a dark brown material, which was transferred to a mould and cured at different temperatures. Motaung and co-workers [33] first prepared a catalyst by dissolving 0.6 g of p-toluenesulfonic acid monohydrate in 10 mL of deionized water. Subsequently, the catalyst was added dropwise to FA with continuous stirring and the mixture was left undisturbed at room temperature overnight, until it solidified before curing. In another study, Lems and co-workers [49] investigated the possibility to improve the mechanics of porous cellulose materials through in-situ polymerization of FA. In the study, maleic anhydride was used for FA polymerization, followed by an in-situ polymerization process.

2.3. Thermal properties

Thermal stability is one of the most significant properties of polymeric materials, since it is often a limiting factor in both processing and end-use applications. Motaung et al. [45] observed a significant increase in thermal stability of sodium hypochlorite and potassium hydroxide treated cotton fibres, compared to sodium hydroxide treated cotton fibres. The increase in thermal stability was associated with the removal of hemicelluloses, waxes and pectin from the cellulose material, as these components have lower thermal stability, compared to cellulose. When the same cellulose was incorporated in PFA, they reported increased thermal stability. Two thermal degradation steps are visible on the DTG curves (Fig. 2.3). The addition of treated flax fibre generally increases the thermal stability of composites, while poor interfacial interaction leads to low thermal stability of untreated samples. However, it has been reported that hemicelluloses and lignin in natural fibres could also catalyse the thermal degradation of natural fibre-based composites [52].

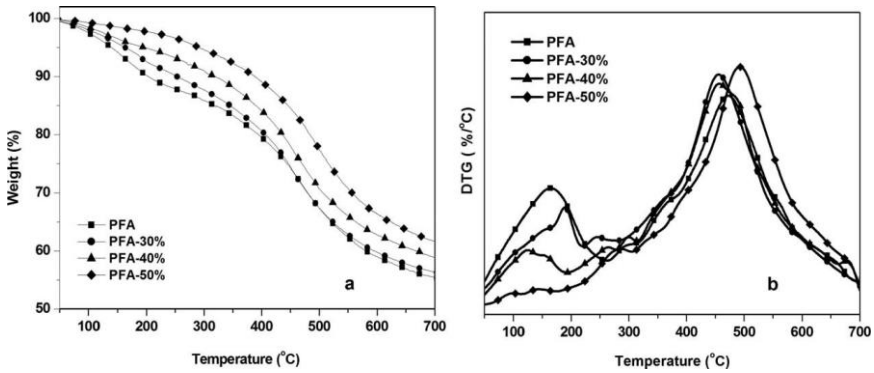

Figure 2.3: TGA and DTG curves of pure PFA, PFA containing 30, 40 and 50% acid hydrolysed cellulose [33].

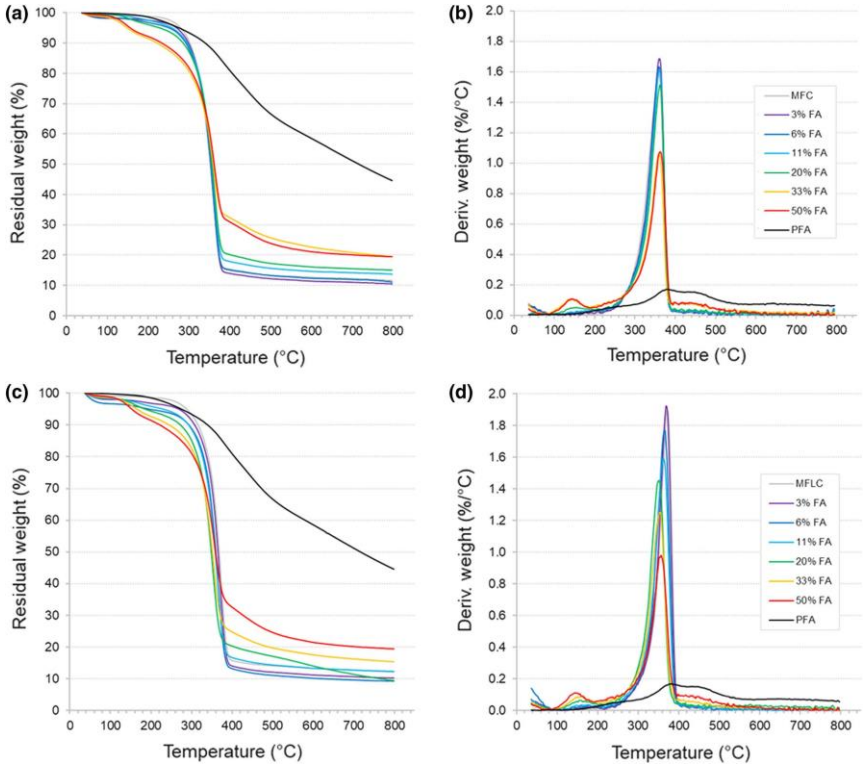

Figure 2.4: TGA and DTG curves of MFC (a and b), MFLC (c and d) of composites comprising different amounts of FA [49].

Pranger et al. [43] and Ahmad et al. [32] reported increased thermal stability of PFA-based nanocomposites, although they used different preparation methods and cellulose source materials. Both studies showed two thermal degradation steps due to the formation of alkyl

furans and scission of furanic links to form ketonic volatile compounds. In another study, nanocomposites reinforced with 1 wt% sisal whiskers showed a slightly higher thermal stability, compared to those incorporating 2 wt%. Also, a gradual increase in the thermal stability of cellulose PFA nanocomposites was observed with the increase in acid concentrations in hydrolysis [34].

Lems et al [49] observed significant changes in thermal stability associated with the increase in polymerized FA content in porous structures (Fig. 2.4). Both pure microfibrillated cellulose (MFC) and microfibrillated lignocellulose (MFLC) display a distinctive sigmoidal decomposition curve, with rapid decomposition starting at temperatures of around 342 °C (MFLC) and 320 °C (MFC). Hence, MFLC is more thermally stable compared to MFC. This can be explained by the higher crystallinity index of MFLC (0.74), compared to MFC (0.70), as well as/or the degree of polymerization due to dissimilar sources and processing conditions. The shape of the curves deviates to a steadier decomposition behaviour, typical of pure PFA, with an increasing amount of FA. The DTG curves (Fig. 2.4 a and b) of both compounds and neat PFA comprising at least 33% FA display an unblemished shoulder at temperatures above 400 °C, which is related to the scission of furan rings. The composites containing cellulose fibres illustrate sharp decomposition peaks, in contrast to the neat PFA. It is evident that the materials with higher FA content have a lower thermal decomposition rate and unreacted FA is released at a higher rate around 150 °C.

2.4. Mechanical properties

The mechanical properties of cellulose PFA nanocomposites are generally investigated using the dynamic mechanical spectroscopy (DMA) technique. The incorporation of cellulose nanocrystals into the polymer matrix has shown to significantly improve the storage modulus. Moreover, there was lowered intensity of the tan δ peaks related to improved elasticity of the matrix and reduced energy losses due to the introduction of the nanocrystals [32]. Similar results have been reported by Pranger and co-workers, [35] with a significant increase in the storage modulus of the PFA nanocomposite at low filler content. This was apparently related to the strong reinforcement effect of a well dispersed high-specific surface nanofiller in FA during the sonication step. The same effect was observed during the polymerization step of FA, resulting in higher values of the storage modulus of the cellulose PFA nanocomposites. In a

similar study conducted by Motaung and co-workers, [33] where different acid concentrations were used during the hydrolysis step, the storage modulus of the materials corresponding to 50% sulphuric acid was the lowest, compared to other samples, while the highest was achieved for 30% acid hydrolysis (Fig. 2.5). This effect was attributed to poor interfacial adhesion of cellulose and PFA obtained as a result of using higher acid content.

Figure 2.5 (b) shows that the presence of the whiskers decreased the intensity of the damping factor. This effect proves that the introduction of nanocrystals improves the elasticity of the matrix, while reducing the energy loss. Tan delta curves (Tα) are known to be more accurate for glass transition temperature (Tg) of the matrix [53]. Motaung et al. [33] observed a positional shift for the 30% acid hydrolysed cellulose nanocomposites from lower to higher temperature, when compared to the pure PFA. This was associated with effective immobilization of the polymer chains, taking place at the lowest acid concentration, which complements the observed increase in rigidity [45]. Similar observations have been made in the studies of Ahmad et al. [50] and Motaung et al. [34].

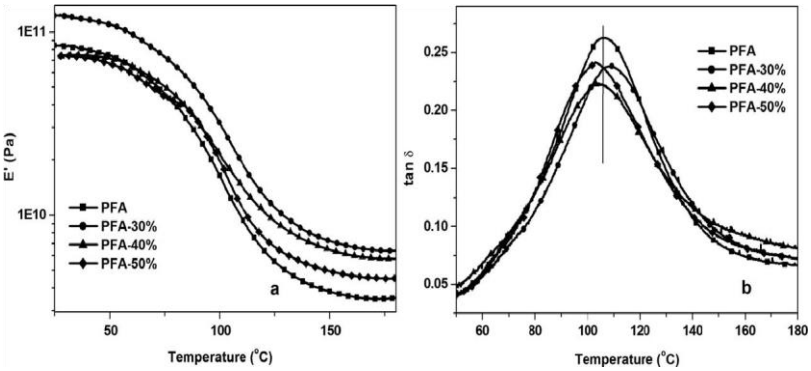

Figure 2.5: DMA results for (a) storage modulus and (b) tan δ curves of pure PFA and cellulose PFA nanocomposites as a function of temperature [33].

Moreover, in the study by Motaung et al., [34] it was observed that the addition of fibres led to an increase in the storage modulus, compared to that of the neat PFA, predominantly at temperatures above 70 °C. The highest storage modulus has been observed for the composite containing 1.5% treated fibre. The 2% treated fibre containing composite unexpectedly revealed the lowest storage modulus, compared to all the other composites investigated in the cited work. The increase in storage modulus has been attributed to the reinforcement with flax

fibre. Flexural properties have been also shown to be strongly enhanced due to the presence of flax fibres in PFA composites, but as a function of the alkali concentration used during the treatment of the fibre [48]. Thus, the flexural strength of 1.5% and 2% treated fibre composites displayed the best flexural strength, by approximately 10% higher than that of pure PFA. This may be due to the bonding of flax fibre with the PFA matrix, which provided good fibre–matrix interaction. The low flexural strength of untreated fibre composites and those incorporating fibre treated with low alkaline concentration is caused by the poor interfacial interaction, which does not impart enough strength to composite to endure the applied flexural stress. However, other researchers have stated that alkalization at higher concentrations is likely to degrade cellulose to a certain degree [54-56].

2.5. Morphological characteristics

Various microscopic techniques, such as scanning electron microscopy (SEM) and transmission electron microscopy (TEM), are used to thoroughly study the morphology of composites. Figure 2.6 shows the fractured surface of PFA nanocomposites incorporating nanocellulose obtained with various acid concentrations in hydrolysis. The filler is homogenously dispersed in the polymer matrix, though it tends to group into agglomerates [33] Roghani-Mamaqani and co-workers [30] made similar observations. The surface microscopy images of cellulose PFA nanocomposites did not reveal visible fibres, suggesting good dispersion.

In other studies, TEM micrographs of novolak/grapheme FA composites revealed light and dark shades (the rough nanosheet of graphene/FA), which also proved homogenous dispersion [33-35] On the contrary, in a study by Deka et al., micrographs revealed broken fibres and fibre pull-out for kenaf composites with low loading of fibres (Fig. 2.7) [31].

In the mentioned work, the researchers used hydrogen peroxide for fibre treatment instead of an acid, which explains the fibre pull-outs. Higher concentrations showed more broken fibres. Fibre pull-outs may also be caused by poor interfacial interaction, as shown in the SEM analysis of fractured surfaces of PFA composites in another study [34]. PFA composites show

a cluster of fibres that look broken in the polymeric matrix. This phenomenon is directly related to the interaction between the natural fibre and the polymer matrix.

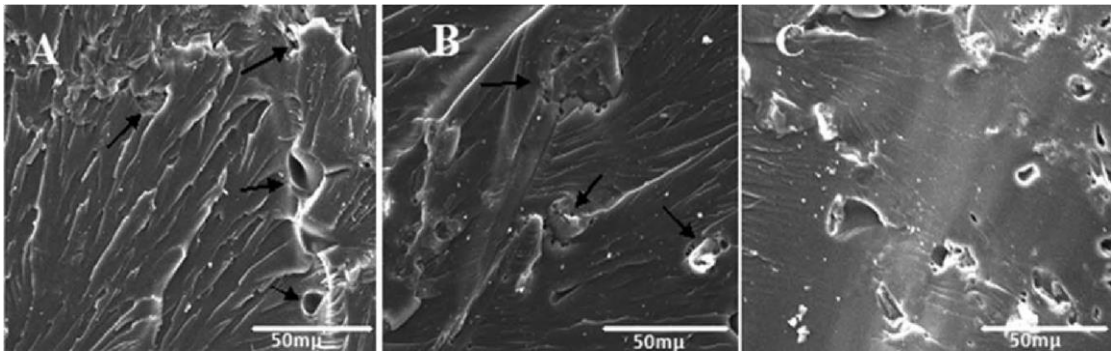

Figure 2.6: Fracture surface of PFA nanocomposites incorporating nanocellulose obtained after (a) 30, (b) 40 and (c) 50% acid hydrolysis [34].

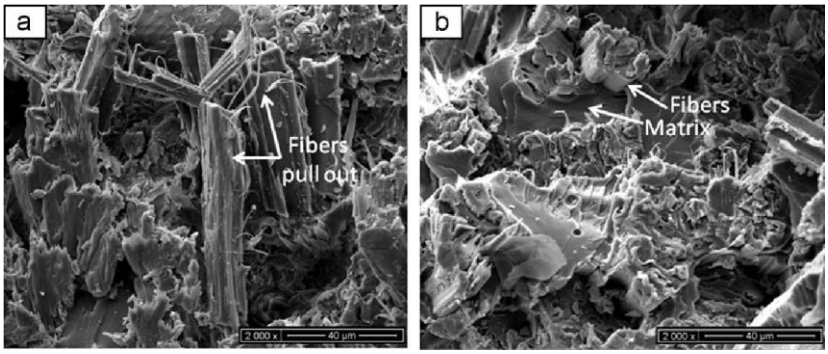

Figure 2.7: SEM images of (a) impact fractured surface, (b) tensile fractured surface of PFA/Kenaf 20% [31].

2.6. Conclusion

Cellulose PFA nanocomposites generally require low filler content for yielding increased thermal stability and mechanical properties. The thermal stability results showed a significant increase when treated fibre was utilized, compared to untreated fibre. Thermal stability is also influenced by an increase in acid concentrations used in hydrolysis and the amount of polymerized FA. As a matter of fact, since the majority of PFA uses are in high temperature applications, due to its flame retardancy, high char yield and low smoke release, the thermal stability of the developed composites is critical.

The incorporation of cellulose nanocrystals into the polymer matrix has shown to significantly improve both the storage modulus and flexural strength, while reducing the intensity of tan δ peaks. This effect proves that the introduction of nanocrystals improves the elasticity of the matrix, while reducing the energy loss. The storage modulus and flexural strength are influenced by the type of acid used during hydrolysis and its concentration. Morphological analysis results have also revealed the influence of the acid type and content used during the hydrolysis treatment.

Researchers have been investigating the most suitable acid for the extraction of cellulose nanocrystals for decades. Thus, many have used sulphuric acid in various concentrations for this purpose, while others have resorted to hydrochloric acid as their acid of choice. There has been also reported the use of phosphoric acid and hydrobromic acid, as well as ionic liquids, but nanocelluloses obtained by these methods have not yet been investigated in PFA composites. This could be an interesting opportunity to expand the research on cellulose PFA nanocomposites. Another interesting phenomenon that deserves thorough attention could be the effect of reinforcing PFA nanocomposites with nanocelluloses obtained by acid mixtures, because in the literature, it has been highlighted those different acids yield different cellulosic morphology.

2.7. References

1. Brinchi, L., et al., *Production of nanocrystalline cellulose from lignocellulosic biomass: technology and applications.* Carbohydrate Polymers, 2013. **94**(1): p. 154-169.
2. Huber, T., et al., *A critical review of all-cellulose composites.* Journal of Materials Science, 2012. **47**(3): p. 1171-1186.
3. Hamelinck, C.N., G. Van Hooijdonk, and A.P. Faaij, *Ethanol from lignocellulosic biomass: techno-economic performance in short-, middle-and long-term.* Biomass and bioenergy, 2005. **28**(4): p. 384-410.
4. Mohanty, A.K., M. Misra, and L. Drzal, *Sustainable bio-composites from renewable resources: opportunities and challenges in the green materials world.* Journal of Polymers and the Environment, 2002. **10**(1-2): p. 19-26.
5. Cotana, F., et al., *NANOCRYSTALLINE CELLULOSE FROM LIGNOCELLULOSIC BIOMASS: APPLICATIONS AND FUTURE PROSPECTS.*
6. Biagiotti, J., D. Puglia, and J.M. Kenny, *A review on natural fibre-based composites-part I: structure, processing and properties of vegetable fibres.* Journal of Natural Fibres, 2004. **1**(2): p. 37-68.
7. Cherian, B.M., et al., *Isolation of nanocellulose from pineapple leaf fibres by steam explosion.* Carbohydrate Polymers, 2010. **81**(3): p. 720-725.
8. Miao, C. and W.Y. Hamad, *Cellulose reinforced polymer composites and nanocomposites: a critical review.* Cellulose, 2013. **20**(5): p. 2221-2262.
9. Sakurada, I., Y. Nukushina, and T. Ito, *Experimental determination of the elastic modulus of crystalline regions in oriented polymers.* Journal of Polymer Science Part A: Polymer Chemistry, 1962. **57**(165): p. 651-660.
10. Moon, R.J., et al., *Cellulose nanomaterials review: structure, properties and nanocomposites.* Chemical Society Reviews, 2011. **40**(7): p. 3941-3994.
11. Hubbe, M.A., et al., *Cellulosic nanocomposites: a review.* BioResources, 2008. **3**(3): p. 929-980.
12. Siqueira, G., J. Bras, and A. Dufresne, *Cellulosic bionanocomposites: a review of preparation, properties and applications.* Polymers, 2010. **2**(4): p. 728-765.

13. Hamad, W., *On the development and applications of cellulosic nanofibrillar and nanocrystalline materials.* The Canadian Journal of Chemical Engineering, 2006. **84**(5): p. 513-519.
14. Cheng, M., W. Chen, and T. Weerasooriya, *Experimental investigation of the transverse mechanical properties of a single Kevlar® KM2 fibre.* International Journal of Solids and Structures, 2004. **41**(22-23): p. 6215-6232.
15. Nishino, T., I. Matsuda, and K. Hirao, *Cellulose self-reinforced composite.* ecocomposites, University of London, 2003.
16. O'sullivan, A.C., *Cellulose: the structure slowly unravels.* Cellulose, 1997. **4**(3): p. 173-207.
17. Chen, W., G.C. Lickfield, and C.Q. Yang, *Molecular modeling of cellulose in amorphous state. Part I: model building and plastic deformation study.* Polymer, 2004. **45**(3): p. 1063-1071.
18. Nishino, T., K. Takano, and K. Nakamae, *Elastic modulus of the crystalline regions of cellulose polymorphs.* Journal of Polymer Science Part B: Polymer Physics, 1995. **33**(11): p. 1647-1651.
19. Gandini, A., *Furans as offspring of sugars and polysaccharides and progenitors of a family of remarkable polymers: a review of recent progress.* Polymer Chemistry, 2010. **1**(3): p. 245-251.
20. Belgacem, M.N. and A. Gandini, *Materials from vegetable oils: major sources, properties and applications*, in *Monomers, polymers and composites from renewable resources*. 2008, Elsevier. p. 39-66.
21. Gandini, A. and M.N. Belgacem, *Furans in polymer chemistry.* Progress in Polymer Science, 1997. **22**(6): p. 1203-1379.
22. Moreau, C., M.N. Belgacem, and A. Gandini, *Recent catalytic advances in the chemistry of substituted furans from carbohydrates and in the ensuing polymers.* Topics in Catalysis, 2004. **27**(1-4): p. 11-30.
23. Choura, M., N.M. Belgacem, and A. Gandini, *Acid-catalyzed polycondensation of furfuryl alcohol: Mechanisms of chromophore formation and cross-linking.* Macromolecules, 1996. **29**(11): p. 3839-3850.
24. Principe, M., P. Ortiz, and R. Martínez, *An NMR study of poly (furfuryl alcohol) prepared with p-toluenesulphonic acid.* Polymer international, 1999. **48**(8): p. 637-641.
25. González, R., J.M. Figueroa, and H. González, *Furfuryl alcohol polymerisation by iodine in methylene chloride.* European Polymer Journal, 2002. **38**(2): p. 287-297.

26. Song, C., T. Wang, and J. Qiu, *Preparation of C/CMS composite membranes derived from Poly (furfuryl alcohol) polymerized by iodine catalyst.* Desalination, 2009. **249**(2): p. 486-489.
27. Cesano, F., et al., *Synthesis of ZnO–carbon composites and imprinted carbon by the pyrolysis of ZnCl2-catalyzed furfuryl alcohol polymers.* Journal of Photochemistry and Photobiology A: Chemistry, 2008. **196**(2-3): p. 143-153.
28. Wang, H. and J. Yao, *Use of poly (furfuryl alcohol) in the fabrication of nanostructured carbons and nanocomposites.* Industrial & engineering chemistry research, 2006. **45**(19): p. 6393-6404.
29. Trindade, W.G., et al., *Phenolic thermoset matrix reinforced with sugar cane bagasse fibres: attempt to develop a new fibre surface chemical modification involving formation of quinones followed by reaction with furfuryl alcohol.* Macromolecular Materials and Engineering, 2004. **289**(8): p. 728-736.
30. Roghani-Mamaqani, H., et al., *Furfuryl alcohol functionalized graphene nanosheets for synthesis of high carbon yield novolak composites.* Journal of Applied Polymer Science, 2014. **131**(11).
31. Deka, H., M. Misra, and A. Mohanty, *Renewable resource based "all green composites" from kenaf biofibre and poly (furfuryl alcohol) bioresin.* Industrial Crops and Products, 2013. **41**: p. 94-101.
32. Ahmad, E., A. Luyt, and V. Djoković, *Thermal and dynamic mechanical properties of bio-based poly (furfuryl alcohol)/sisal whiskers nanocomposites.* Polymer bulletin, 2013. **70**(4): p. 1265-1276.
33. Motaung, T., et al., *The effect of acid content on the poly (furfuryl) alcohol/cellulose composites.* Polymer Composites, 2016. **37**(8): p. 2434-2441.
34. Motaung, T.E., et al., *Agave and sisal fibre-reinforced polyfurfuryl alcohol composites.* Journal of Thermoplastic Composite Materials, 2017. **30**(10): p. 1323-1343.
35. Pranger, L.A., G.A. Nunnery, and R. Tannenbaum, *Mechanism of the nanoparticle-catalyzed polymerization of furfuryl alcohol and the thermal and mechanical properties of the resulting nanocomposites.* Composites Part B: Engineering, 2012. **43**(3): p. 1139-1146.
36. Chazeau, L., et al., *Viscoelastic properties of plasticized PVC reinforced with cellulose whiskers.* Journal of Applied Polymer Science, 1999. **71**(11): p. 1797-1808.
37. Dufresne, A., M.B. Kellerhals, and B. Witholt, *Transcrystallization in Mcl-PHAs/cellulose whiskers composites.* Macromolecules, 1999. **32**(22): p. 7396-7401.

38. Luo, J.-J. and I.M. Daniel, *Characterization and modeling of mechanical behavior of polymer/clay nanocomposites.* Composites science and technology, 2003. **63**(11): p. 1607-1616.
39. Terech, P., L. Chazeau, and J. Cavaille, *A small-angle scattering study of cellulose whiskers in aqueous suspensions.* Macromolecules, 1999. **32**(6): p. 1872-1875.
40. Alexandre, M. and P. Dubois, *Polymer-layered silicate nanocomposites: preparation, properties and uses of a new class of materials.* Materials Science and Engineering: R: Reports, 2000. **28**(1-2): p. 1-63.
41. Dubief, D., E. Samain, and A. Dufresne, *Polysaccharide microcrystals reinforced amorphous poly (β-hydroxyoctanoate) nanocomposite materials.* Macromolecules, 1999. **32**(18): p. 5765-5771.
42. Naik, S.N., et al., *Production of first and second generation biofuels: a comprehensive review.* Renewable and sustainable energy reviews, 2010. **14**(2): p. 578-597.
43. Hayes, D.J., *An examination of biorefining processes, catalysts and challenges.* Catalysis Today, 2009. **145**(1-2): p. 138-151.
44. Beck-Candanedo, S., M. Roman, and D.G. Gray, *Effect of reaction conditions on the properties and behavior of wood cellulose nanocrystal suspensions.* Biomacromolecules, 2005. **6**(2): p. 1048-1054.
45. Elazzouzi-Hafraoui, S., et al., *The shape and size distribution of crystalline nanoparticles prepared by acid hydrolysis of native cellulose.* Biomacromolecules, 2007. **9**(1): p. 57-65.
46. Favier, V., et al., *Nanocomposite materials from latex and cellulose whiskers.* Polymers for Advanced Technologies, 1995. **6**(5): p. 351-355.
47. Habibi, Y., L.A. Lucia, and O.J. Rojas, *Cellulose nanocrystals: chemistry, self-assembly, and applications.* Chemical reviews, 2010. **110**(6): p. 3479-3500.
48. Motaung, T.E., M.E. Mngomezulu, and M.J. Hato, *Effects of alkali treatment on the poly (furfuryl) alcohol–flax fibre composites.* Journal of Thermoplastic Composite Materials, 2018. **31**(1): p. 48-60.
49. Lems, E.-M., et al., *Reinforcing effect of poly (furfuryl alcohol) in cellulose-based porous materials.* Cellulose, 2019. **26**(7): p. 4431-4444.
50. Park, S., et al., *Cellulose crystallinity index: measurement techniques and their impact on interpreting cellulase performance.* Biotechnology for biofuels, 2010. **3**(1): p. 10.

51. Roman, M. and W.T. Winter, *Effect of sulfate groups from sulfuric acid hydrolysis on the thermal degradation behavior of bacterial cellulose.* Biomacromolecules, 2004. **5**(5): p. 1671-1677.
52. Mwaikambo, L.Y. and M.P. Ansell, *Chemical modification of hemp, sisal, jute, and kapok fibres by alkalization.* Journal of applied polymer science, 2002. **84**(12): p. 2222-2234.
53. Azizi Samir, M.A.S., et al., *Preparation of cellulose whiskers reinforced nanocomposites from an organic medium suspension.* Macromolecules, 2004. **37**(4): p. 1386-1393.
54. Rong, M.Z., et al., *The effect of fibre treatment on the mechanical properties of unidirectional sisal-reinforced epoxy composites.* Composites Science and technology, 2001. **61**(10): p. 1437-1447.

CHAPTER 3

THE EFFECT OF H_2SO_4/$HClO_4$ MIXED ACID CONCENTRATION ON PROPERTIES OF CELLULOSE NANOCRYSTALS FROM SUGARCANE BAGASSE (SCB)

(Article Submitted and Accepted for Publication by Wood Research Journal)

3.1. Introduction

Recently, cellulose nanocrystals (CNCs) have attracted attention due to their significant abundance, renewability properties, low density and high reinforcing capabilities etc. [1, 2]. Hence, they have also attracted significant applications in food packaging, cosmetics, polymers, biomedical amongst others [3-7]. Interestingly, the properties of CNCs are influenced by the choice of extraction method and the source of cellulosic material used [2]. Furthermore, the isolation of CNCs is affected by reaction time, reaction temperature and the ratio of acid to fiber or cellulose [8]. CNCs can be extracted through different methods including mechanical, enzymatic hydrolysis and acid hydrolysis treatment. However, acid hydrolysis is by far the widely used treatment of CNC isolation, particularly sulphuric acid (H_2SO_4) hydrolysis [9, 10]. This might probably due stable suspension with high yield and crystallization produced, because of the sulphate ions [11, 12]. On the contrary, CNCs isolated through H_2SO_4 hydrolysis produces suspensions with low thermal stability [13, 14]. Therefore, many researchers have investigated acid hydrolysis using other acids such as HCl, H_3PO_4, HBr, HNO_3, etc. [15-17]. It has been discovered that CNCs extracted from these acids aggregate easily due to the abundance of surface hydroxyl groups which form strong intra-and inter-molecular hydrogen bonding interaction [18, 19]. In a study conducted by Correa et. al. it was observed that the rate of fibre aggregation increased with the increase in HCl concentration [20]. However, the resultant CNCs showed improved thermal properties when compared to H_2SO_4 hydrolysed CNCs. These two discoveries were due to the decrease in sulphate ions.

Therefore, the focus has shifted to the use of acid mixtures to isolate CNCs [20-22]. The resultant CNCs typically showed excellent reinforcing properties in polymer nanocomposites manufacturing. Furthermore, they showed excellent dispersion in several organic solvents such as ethanol. The isolation of CNCs using HCOOH/HCl interestingly showed improved thermal and crystallinity properties due to the introduction of formate groups in a study by Kassab, Z., et al [23]. Moreover, it was apparent from the study that reinforcing, and the reducibility are dependent on the capability formate group, thermal stability and crystallinity of CNCs. Maciel et. al. [24] investigated the effect of acid hydrolysis conditions of 50 wt%, 60 wt% and 64 wt% of sulphuric acid. Among these three acid concentrations, the optimal properties were observed when using 64 wt% acid hydrolysis. However, in another study by Pan et. al. [16] it was discovered that an increase in acid concentration from 20 to 60 wt% led to the breakage of

CNCs fibres and produced suspension with lower crystallinity. It is apparent that the choice of acids used, and the acid concentration have an effect in the properties of the resultant CNCs. In this study, the effect of sulphuric acid mixed with perchloric acid ($HClO_4$) with varying acid concentration from 45 wt%, 55 wt% and 65 wt% was investigated. The thermal and morphological properties of H_2SO_4/$HClO_4$ hydrolysed CNCs extracted from sugarcane bagasse were determined.

3.2. Materials and Methods

3.2.1. Materials

Sugarcane bagasse (SCB) waste was supplied by the sugar company at Empangeni (Felixton) in KwaZulu Natal, South Africa. Sodium hydroxide (NaOH) 99.9%, sodium hypochlorite ($NaClO_2$) 80%, glacial acetic acid (CH_3COOH), sulphuric acid (H_2SO_4) 95-99%, and perchloric acid ($HClO_4$) 60% were purchased at Merck chemicals and used without being purified.

3.2.2. Extraction of cellulose

SCB was mechanically grounded using a Fritsch cutting mill pulveriser 15. The SCB was then boiled with distilled water for 2 hours and left in the oven to dry overnight at 55°C. The dried SCB was chemically treated with 4 wt% NaOH at 80 °C for 1 hour followed by rinsing with distilled water. The process was repeated 2 times. The alkali treated SCB was then left in an oven to dry at 55°C overnight. The dried alkali treated SCB was then bleached using a buffer solution (54g of NaOH and 150 ml of CH_3COOH mixed with 2L of 1.7wt% solution of the $NaClO_2$ solution) for an hour at 80°C; this step was repeated 2 times. Finally, the bleached cellulose was filtered, washed with distilled water until a neutral pH was reached and dried overnight at 55°C.

3.2.3. Extraction of cellulose nanocrystals

The dried cellulose sample was finely crushed in a Fritsch cutting mill Pulveriser 15. A finely dried mass of 15g of cellulose was weighed in 5 separate 600 ml beakers. A concentration of 45%, 55%, 65% H_2SO_4/$HClO_4$ mixture of acid and a 65% H_2SO_4 were prepared. A volume of

250 ml of 45% H_2SO_4/$HClO_4$ was added to a beaker in an ice bath of 10°C and stirred with a mechanical stirrer for 30 minutes. The reaction was then quenched with distilled water and left overnight. The mixture was then subjected to a centrifuge for 15 minutes. Subsequent, dialysis against distilled water was executed for 5 days until pH was neutral. Finally, the CNCs were then dried in an oven over 5 days at 30°C. The same procedure was repeated for other acid concentrations.

3.3. Characterization Methods

3.3.1. Fourier Transform Infra-Red Spectroscopy

Perkin Elmer attenuated total reflection FTIR spectrometer (Perkin Elmer UATR Two) operated in the diffuse reflectance mode was used to investigate structural functional groups of polymer samples. The spectral region between 4000 and 500 cm^{-1} was used during sample analysis.

3.3.2. X-ray Diffraction

The X-ray diffraction (XRD) samples were characterized on a Bruker AXS Advance D8 diffractometer, Karsruhe, Germany equipped with monochromatic Cu Kα (λ = 1.5406 Å) as X-ray source operating at 40 KV and 40 mA at room temperature. The crystallinity index (CI) was computed using both the Segal empirical method and deconvolution method. The Segal empirical method is calculated from the height of I_{002} and the height of I_{min} between the 002 peak and the 001 peak. The CI was calculated using the method below.

$$CI\ \% = \frac{I_{002} - I_{am}}{I_{002}} \times 100 \qquad (1)$$

Where, I_{002} denotes the maximum intensity of diffraction of the 002 peak while I_{am} denotes the intensity of diffraction of the amorphous material.

Using the deconvolution method, the CI is determined using the ratio of the area of all crystalline peaks to the total area.

$$CI\ \% = \frac{\Sigma A_{cryst}}{\Sigma A_{cryst} + \Sigma A_{amorp}} \times 100 \quad (2)$$

Where, A_{cryst} denotes the area of crystalline domain and A_{amorp} denotes the area of the amorphous domain [25].

3.3.3. Scanning Electron Microscopy

FEI Quanta 200 electron microscopy operated at an accelerating voltage of 20KV was used to investigate the morphological properties of the polymer materials studied. The samples were carbon-coated before analysis, using Edward's E306A coating system.

3.3.4. Thermogravimetric Analysis

For the thermogravimetric analysis (TGA), the analysis was conducted using TGA analyser (Perkin Elmer Pyris 6). Samples ranging from 10-15 mg were heated at a temperature range 35 to 800°C at a heating rate of 5°C per minute under nitrogen environment at a flow rate of 20 ml min^{-1}.

3.4. Results and Discussion

3.4.1. FTIR spectroscopy analysis

The FTIR was employed to better understand the functional groups associated with CNCs after acid hydrolysis. The FTIR spectra of raw SCB, cellulose, H_2SO_4/$HClO_4$ hydrolysed CNCs (using 45%, 55% and 65% concentration of acid) and 45% H_2SO_4 hydrolysed CNCs are presented in Figure 3.1. The raw SCB showed characteristic of natural fibre with peaks observed at 3327 cm^{-1} (─OH stretching), 2896 cm^{-1} (C─H vibrations), 1361 cm^{-1} (─CH_2 bending), 1028 cm^{-1} (C─O stretching) and 892 cm^{-1} (─CH_2 bending) [26-31]. There was a noticeable addition of a peak at around 1309 cm^{-1} for all CNCs and extracted cellulose spectra which was absent for raw SCB. The peak maybe attributed to the C─H wagging when hydrogen bond was disrupted [32]. In addition, the extracted cellulose showed similar peaks patterns with the raw SCB, with the addition of the peak around 1309 cm^{-1}. However, there was a decrease in peak intensity of peaks around 1434 and 1236 cm^{-1} and the increase in the peak intensity at 892 cm^{-1} which could be attributed to removal of the amorphous regions of cellulosic materials [33, 34]. With regards to the 45% H_2SO_4 hydrolysed CNCs, the peaks appeared to be more pronounced with the absence of the peak at 1557 cm^{-1} when compared to the extracted cellulose which could be

attributed to further removal of the amorphous regions of cellulosic materials [33, 34]. For mixed acid hydrolysis, the 45% and 65% showed similar peak patterns with peaks around 3327 and 2896 cm^{-1} becoming more diminished compared to 55% acid concentrations. With the introduction perchloric acid, there was a removal of the peak around 1636 cm^{-1} attributed to the C=O stretching peak.

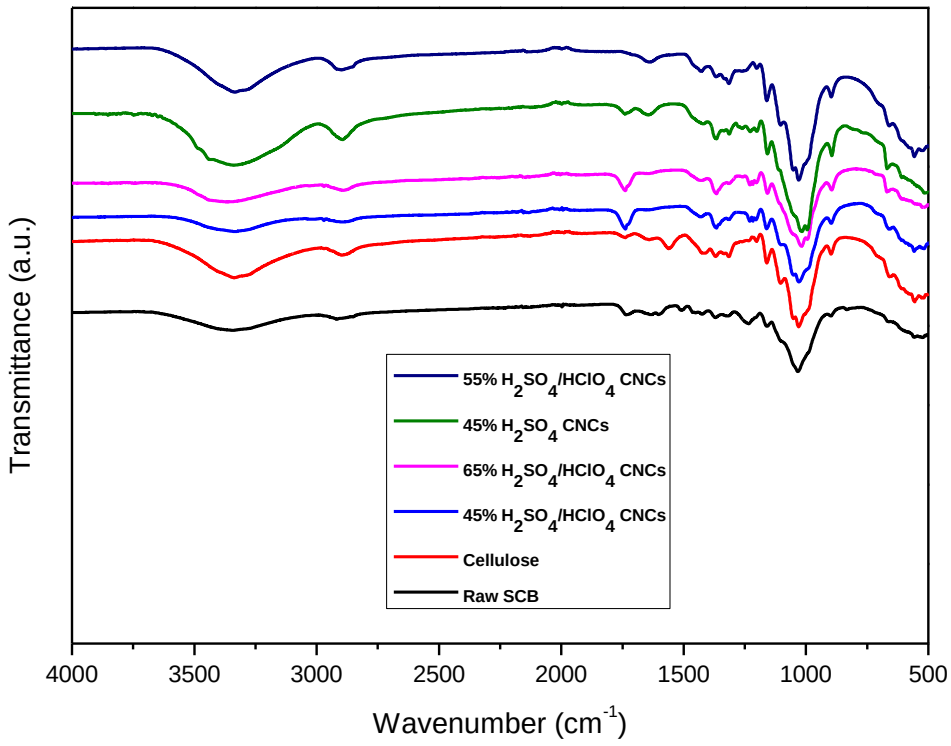

Figure 3.1: FTIR spectra of the raw sugarcane bagasse, cellulose, 45% H_2SO_4 hydrolysed CNCs, 45% $H_2SO_4/HClO_4$ hydrolysed CNCs, 55% $H_2SO_4/HClO_4$ hydrolysed CNCs and 65% $H_2SO_4/HClO_4$ hydrolysed CNCs.

3.4.2. X-*ray* diffraction analysis

The XRD spectra of raw SCB, extracted cellulose, $H_2SO_4/HClO_4$ hydrolysed CNCs (using 45%, 55% and 65% concentration of acid) and 45% H_2SO_4 hydrolysed CNCs are shown in Figure 3.2. The raw SCB material displayed peaks at 2θ = 15, 23 and 35°, typical of lignocellulosic material [25]. Moreover, the extracted cellulose showed similar behaviour compared to raw SCB with more pronounced peaks. Interestingly, the 45% H_2SO_4 hydrolysed CNCs and 65% $H_2SO_4/HClO_4$ hydrolysed CNCs displayed similar peaks at 2θ = 12, 20, 22 and 35°. However, the 55% $H_2SO_4/HClO_4$ hydrolysed CNCs displayed more pronounced peaks compared to 45%

H_2SO_4/$HClO_4$ hydrolysed CNCs. In general, it can be noted that the intensity of the diffraction peak increased after chemical treatment for all the samples. These might be attributed by the removal of non-cellulosic materials such as hemicellulose, lignin and pectin.

Crystallinity index (CI) values were calculated using both the Segal empirical method and deconvolution methods as shown in Table 3.1. Generally, there was a notable increase in the values of CI values for extracted cellulose as compared to raw SCB. It is known that acid hydrolysis of native cellulose result in an increase in crystallinity index due to the removal lignin, hemicellulose and pectin after the chemical treatment [34].

Table 3.1. Crystalline Index values of materials studied using Segal and deconvolution methods.

Fiber type	**CI (%) (Segal)**	**CI (%) (deconvolution)**
Raw SCB	50	32
Cellulose	68	49
45% H_2SO_4 CNCs	72	51
45% H_2SO_4 /$HClO_4$ CNCs	73	53
55% H_2SO_4 /$HClO_4$ CNCs	76	56
65% H_2SO_4 /$HClO_4$ CNCs	74	54

In addition, there was a further increase in CI after 45% H_2SO_4 hydrolysed CNCs which could be attributed to further removal of amorphous regions in CNCs. As for the mixed acid hydrolysis, 55% H_2SO_4 /$HClO_4$ hydrolysed CNCs displayed the highest CI followed by 65% H_2SO_4 /$HClO_4$ hydrolysed CNCs due to the high acidic concentration as well as the acidic strength of perchloric acid. Hence, the removal of the amorphous regions was easily achieved leading to formation of crystallites. The crystallinity index proved to be more favourable towards a 55% mixed acid. This may be due to the formation of strong enough acid to remove the amorphous regions and weak enough not to destroy the crystalline regions.

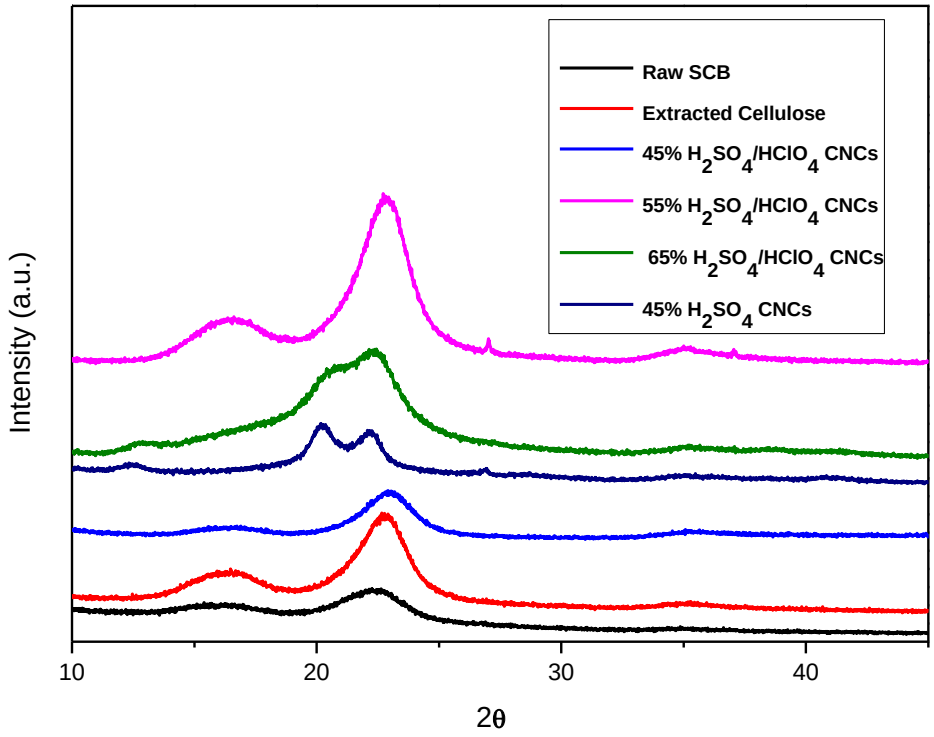

Figure 3.2: XRD spectra of the raw sugarcane bagasse, cellulose, 45% H_2SO_4 hydrolysed CNCs, 45% $H_2SO_4/HClO_4$ hydrolysed CNCs, 55% $H_2SO_4/HClO_4$ hydrolysed CNCs and 65% $H_2SO_4/HClO_4$ hydrolysed CNCs.

3.4.3. Scanning electron microscopy

SEM was conducted to investigate the morphological effect of mixed acid concentration on extracted CNCs. The SEM images of raw SCB, extracted cellulose, 45% H_2SO_4 hydrolysed CNCs, 45% $H_2SO_4/HClO_4$ hydrolysed CNCs, 55% $H_2SO_4/HClO_4$ hydrolysed CNCs and 65% $H_2SO_4/HClO_4$ hydrolysed CNCs are presented in Figure 3.3. In Figure 3.3(a), it can be clearly noticed that there are particles on the surface of the images. These particles are most probably due to the waxes, hemicellulose and pectin present in natural fibers. In addition, there were clearly absent from Figure 3.3(b) as the bleaching removed these amorphous regions as confirmed by both FTIR and crystallinity results. It is also worth noting that extracted cellulose seems to have maintained its rod like structure compared to the rest CNCs which appeared a bit deformed (See arrows). Furthermore, it can be noted that the acid hydrolysis (Figure 3.3(c) to 3.3(e)) did not result in any fibre breakage and pull-outs. These images showed smooth

surface without fibre pull-outs and breakages. Figure 3.3(f) showed characteristics of fibre breakage on the surface. This could be attributed to the high acid concentration. An acid concentration of 65% $H_2SO_4/HClO_4$ is strong enough to cause fibre breakages on the surface of CNCs. The results were further echoed by the crystallinity results. The decrease in CI observed from a 55% compared to a 65% meant the acid concentration is strong enough to cause fibre breakage hence decreasing CI [6].

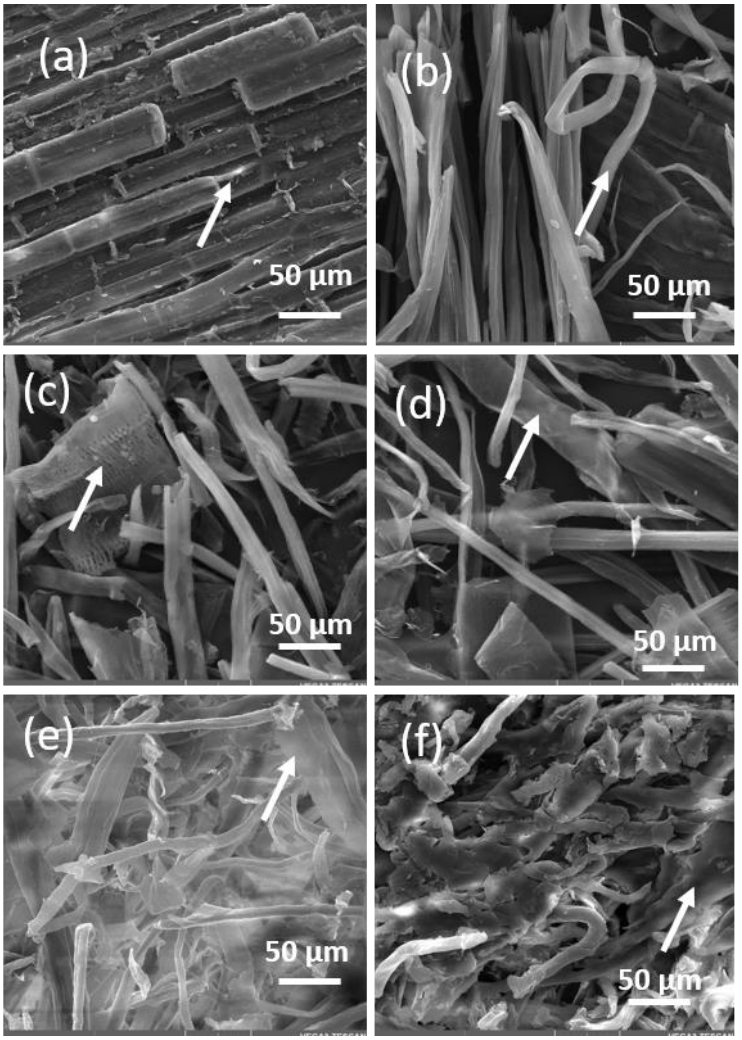

Figure 3.3: SEM images of the (a) the raw sugarcane bagasse, (b) cellulose, (c) 45% H_2SO_4 hydrolysed CNCs, (d) 45% $H_2SO_4/HClO_4$ hydrolysed CNCs, (e) 55% $H_2SO_4/HClO_4$ hydrolysed CNCs and (f) 65% $H_2SO_4/HClO_4$ hydrolysed CNCs.

3.4.4. Thermogravimetric analysis

Thermogravimetric analysis studies were conducted to investigate the influence of acid concentration on the thermal properties of mixture of acids hydrolysed CNCs. The TGA and DTG curves are shown in Figure 3.4 and 3.5 respectively. The raw SCB displayed two degradation steps with the high char content. The first degradation step around 333 °C was attributed to removal of hemicellulose, waxes and pectin and the second degradation step at 492 °C was attributed to lignin degradation [8, 35-37]. However, the extracted cellulose displayed one degradation step at around 337 °C, which was attributed to non-cellulosic materials removal and gradual increase in thermal stability and the highest char content as compared raw SCB [35]. This may be due to the sulphate groups acting as a flame retardant during acid hydrolysis with sulfuric acid. Furthermore, the 45% H_2SO_4 hydrolysed CNCs also displayed one degradation step at 342 °C attributed to complete removal of amorphous regions by acid hydrolysis [38].

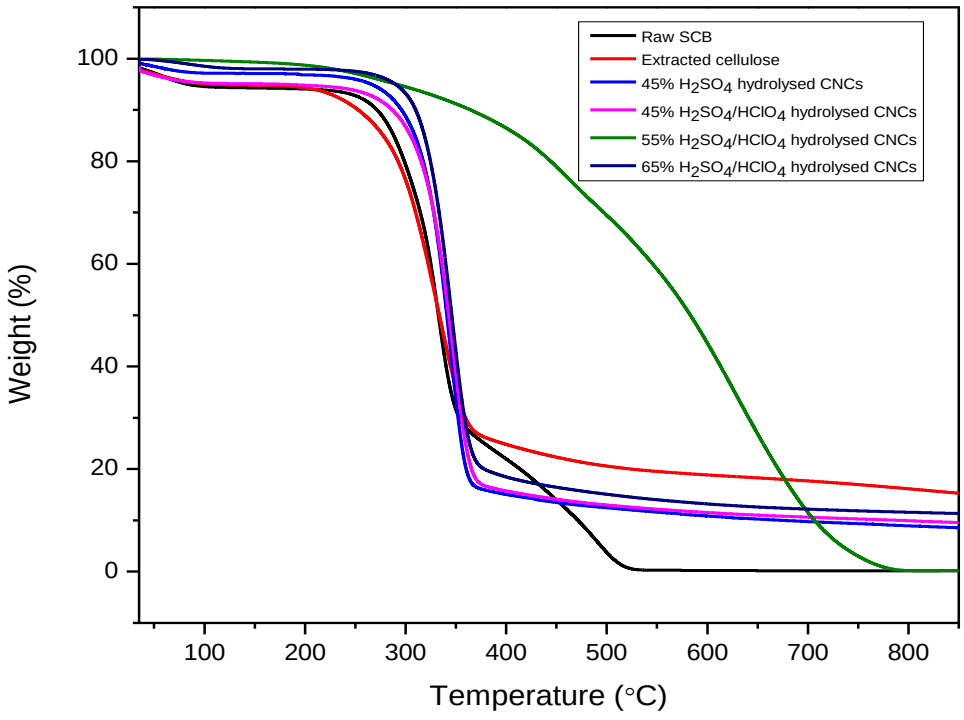

Figure 3.4: TGA curve of the raw sugarcane bagasse, cellulose, 45% H_2SO_4 hydrolysed CNCs, 45% $H_2SO_4/HClO_4$ hydrolysed CNCs, 55% $H_2SO_4/HClO_4$ hydrolysed CNCs and 65% $H_2SO_4/HClO_4$ hydrolysed CNCs.

As for the mixture of acids hydrolysed CNCs, the 45 and 65% acid concentration displayed similar degradation pattern as observed in the FTIR results with one degradation step at 347 °C. However, the 55% acid concentration displayed two degradation steps which are probably attributed to removal of oxygen atoms and the alteration of the furan rings in the condensed aromatic ring respectively. The thermal studies proved to be optimal for 55% $H_2SO_4/HClO_4$ hydrolysed CNCs as it was observed with the crystallinity results. The order of thermal stability was as follows: raw SCB < extracted cellulose < 45% H_2SO_4 hydrolysed CNCs < 65% $H_2SO_4/HClO_4$ hydrolysed CNCs < 45% $H_2SO_4/HClO_4$ hydrolysed CNCs < 55% $H_2SO_4/HClO_4$ hydrolysed CNCs. The 45% H_2SO_4 hydrolysed CNCs displayed the lower thermal stability as compared to other mixture of acids hydrolysed CNCs [13, 14].

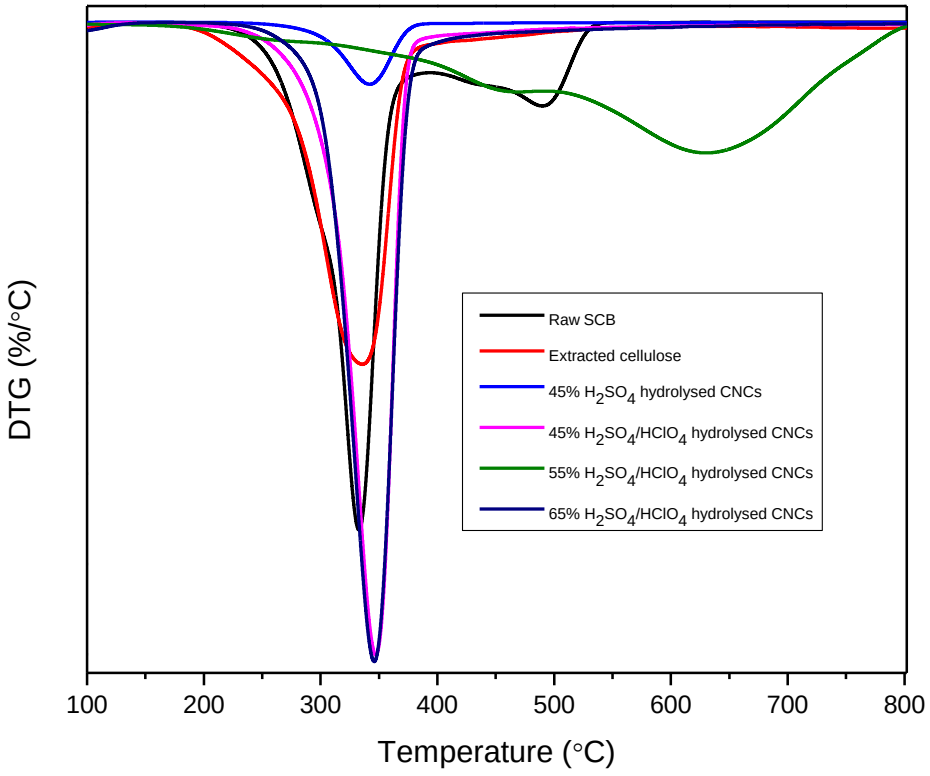

Figure 3.5: DTG curve of the raw sugarcane bagasse, cellulose, 45% H_2SO_4 hydrolysed CNCs, 45% $H_2SO_4/HClO_4$ hydrolysed CNCs, 55% $H_2SO_4/HClO_4$ hydrolysed CNCs and 65% $H_2SO_4/HClO_4$ hydrolysed CNCs.

3.5. Conclusion

The main objective of the study was to investigate the effect of H_2SO_4/$HClO_4$ acid mixture concentration on crystallinity, morphological and thermal properties of the resultant CNCs. The XRD results showed an increase in crystallinity after the extraction of cellulose, with more pronounced results after mix acid hydrolysis. The increase in acid concentration from 45 wt% to 55 wt% resulted in increase in crystallinity index. The crystallinity results were echoed by both the SEM and the thermal studies. The SEM results showed broken fibres for 65 wt% acid concentrations which resulted in decrease in crystallinity index results. The results showed that acid hydrolysis using only H_2SO_4 resulted in lower thermal stability. Though, the addition of $HClO_4$ resultant in improved thermal stability of CNCs.

3.6. References

1. Chen, Y., et al., *Bionanocomposites based on pea starch and cellulose nanowhiskers hydrolyzed from pea hull fibre: effect of hydrolysis time.* Carbohydrate Polymers, 2009. **76**(4): p. 607-615.
2. Oun, A.A. and J.-W. Rhim, *Characterization of nanocelluloses isolated from Ushar (Calotropis procera) seed fiber: Effect of isolation method.* Materials Letters, 2016. **168**: p. 146-150.
3. Hubbe, M.A., et al., *Cellulosic nanocomposites: a review.* BioResources, 2008. **3**(3): p. 929-980.
4. González, M.M., C. Blanco-Tirado, and M.Y. Combariza, *Nanocellulose as an inhibitor of water-in-crude oil emulsion formation.* Fuel, 2020. **264**: p. 116830.
5. Ghafary, S., et al., *Novel morpholine containing cinnamoyl amides as potent tyrosinase inhibitors.* International journal of biological macromolecules, 2019. **135**: p. 978-985.
6. Abd Hamid, S.B., et al., *Synergic effect of tungstophosphoric acid and sonication for rapid synthesis of crystalline nanocellulose.* Carbohydrate polymers, 2016. **138**: p. 349-355.

7. Akkera, H.S., N.N.K. Reddy, and M.C. Sekhar, *Thickness dependent structural and electrical properties of magnetron sputtered nanostructured CrN thin films.* Materials Research, 2017. **20**: p. 712-717.
8. Arserim-Uçar, D.K., et al., *Characterization of bacterial cellulose nanocrystals: Effect of acid treatments and neutralization.* Food Chemistry, 2021. **336**: p. 127597.
9. Habibi, Y., L.A. Lucia, and O.J. Rojas, *Cellulose nanocrystals: chemistry, self-assembly, and applications.* Chemical reviews, 2010. **110**(6): p. 3479-3500.
10. Peng, Y., D.J. Gardner, and Y. Han, *Drying cellulose nanofibrils: in search of a suitable method.* Cellulose, 2012. **19**(1): p. 91-102.
11. Zhong, T., et al., *Nanocellulose from recycled indigo-dyed denim fabric and its application in composite films.* Carbohydrate polymers, 2020. **240**: p. 116283.
12. Cui, S., et al., *Green preparation and characterization of size-controlled nanocrystalline cellulose via ultrasonic-assisted enzymatic hydrolysis.* Industrial Crops and Products, 2016. **83**: p. 346-352.
13. Pandi, N., S.H. Sonawane, and K.A. Kishore, *Synthesis of cellulose nanocrystals (CNCs) from cotton using ultrasound-assisted acid hydrolysis.* Ultrasonics sonochemistry, 2021. **70**: p. 105353.
14. Ji, H., et al., *Strategy towards one-step preparation of carboxylic cellulose nanocrystals and nanofibrils with high yield, carboxylation and highly stable dispersibility using innocuous citric acid.* Green Chemistry, 2019. **21**(8): p. 1956-1964.
15. Yang, X., et al., *Effects of preparation methods on the morphology and properties of nanocellulose (NC) extracted from corn husk.* Industrial Crops and Products, 2017. **109**: p. 241-247.
16. Pan, M., X. Zhou, and M. Chen, *Cellulose nanowhiskers isolation and properties from acid hydrolysis combined with high pressure homogenization.* BioResources, 2013. **8**(1): p. 933-943.
17. Kandhola, G., et al., *Maximizing production of cellulose nanocrystals and nanofibers from pre-extracted loblolly pine kraft pulp: a response surface approach.* Bioresources and Bioprocessing, 2020. **7**(1): p. 1-16.
18. Li, H., et al., *Renoprotective effect and mechanism of polysaccharide from Polyporus umbellatus sclerotia on renal fibrosis.* Carbohydrate polymers, 2019. **212**: p. 1-10.

19. Zheng, D., et al., *Isolation and characterization of nanocellulose with a novel shape from walnut (Juglans regia L.) shell agricultural waste.* Polymers, 2019. **11**(7): p. 1130.
20. Corrêa, A., E. de Morais Teixeira, and L. Pessan, *Mattoso LHCJC (2010).* Cellulose nanofibers from curaua fibers. Cellulose. **17**: p. 1183-1192.
21. Zhang, H., et al., *Effect of silver contents in cellulose nanocrystal/silver nanohybrids on PHBV crystallization and property improvements.* Carbohydrate polymers, 2017. **173**: p. 7-16.
22. Kassab, Z., et al., *Tomato plant residue as new renewable source for cellulose production: extraction of cellulose nanocrystals with different surface functionalities.* Cellulose, 2020. **27**(8): p. 4287-4303.
23. Kassab, Z., et al., *Characteristics of sulfated and carboxylated cellulose nanocrystals extracted from Juncus plant stems.* International journal of biological macromolecules, 2020. **154**: p. 1419-1425.
24. Maciel, M.M.Á.D., et al., *Obtainment and characterization of nanocellulose from an unwoven industrial textile cotton waste: Effect of acid hydrolysis conditions.* International journal of biological macromolecules, 2019. **126**: p. 496-506.
25. Park, S., et al., *Cellulose crystallinity index: measurement techniques and their impact on interpreting cellulase performance.* Biotechnology for biofuels, 2010. **3**(1): p. 1-10.
26. Kalia, S., et al., *Surface modification of plant fibers using environment friendly methods for their application in polymer composites, textile industry and antimicrobial activities: A review.* Journal of Environmental Chemical Engineering, 2013. **1**(3): p. 97-112.
27. Wang, L., R. Kumar, and L. Zhang, *Investigation into hemp fiber-and whisker-reinforced soy protein composites.* Frontiers of Chemistry in China, 2009. **4**(3): p. 313-320.
28. Ahmad, E., A. Luyt, and V. Djoković, *Thermal and dynamic mechanical properties of bio-based poly (furfuryl alcohol)/sisal whiskers nanocomposites.* Polymer bulletin, 2013. **70**(4): p. 1265-1276.
29. Hu, F., et al., *Reinforcement and nucleation of acetylated cellulose nanocrystals in foamed polyester composites.* Carbohydrate polymers, 2015. **129**: p. 208-215.

30. Lani, N., et al., *Isolation, characterization, and application of nanocellulose from oil palm empty fruit bunch fiber as nanocomposites.* Journal of Nanomaterials, 2014. **2014**.
31. Kunaver, M., A. Anžlovar, and E. Žagar, *The fast and effective isolation of nanocellulose from selected cellulosic feedstocks.* Carbohydrate Polymers, 2016. **148**: p. 251-258.
32. Abidi, N., E. Hequet, and L. Cabrales, *Applications of Fourier transform infrared spectroscopy to study cotton fibers.* Fourier transforms—new analytical approaches and FTIR strategies, 2011: p. 89-114.
33. Motaung, T., et al., *The effect of acid content on the poly (furfuryl) alcohol/cellulose composites.* Polymer composites, 2016. **37**(8): p. 2434-2441.
34. Motaung, T.E., et al., *Agave and sisal fibre-reinforced polyfurfuryl alcohol composites.* Journal of Thermoplastic Composite Materials, 2017. **30**(10): p. 1323-1343.
35. Mortari, D., M. Britto, and P. Crnkovic, *Correlation between activation energy and thermal decomposition yield of sugar cane bagasse under CO 2/O 2 and N 2/O 2.* Chemical Engineering Transactions, 2014. **37**: p. 31-36.
36. Roman, M. and W.T. Winter, *Effect of sulfate groups from sulfuric acid hydrolysis on the thermal degradation behavior of bacterial cellulose.* Biomacromolecules, 2004. **5**(5): p. 1671-1677.
37. Petrik, L.F., C. Abiaziem, and A.B. Williams, *Isolation and characterisation of cellulose nanocrystal obtained from sugarcane peel.* 2020.
38. Chen, Z., et al., *Characteristics and kinetic study on pyrolysis of five lignocellulosic biomass via thermogravimetric analysis.* Bioresource technology, 2015. **192**: p. 441-450.

CHAPTER 4

MORPHOLOGY AND THERMAL PROPERTIES COMPARISON OF GREEN EXTRACTED AND ACETYLATED CNCS FROM MAIZE STALK

(*Article submitted and under review by Polymer Composites*)

4.1. Introduction

Of late, cellulose nanocrystal (CNC) has recently received a lot of attention due to its availability, strong mechanical qualities, renewability properties, low density, biodegradability, and high reinforcing capabilities, [1, 2]. As a result, they have piqued interest in food packaging, cosmetics, polymers, and biological applications [3-7]. Both the extraction process utilized, and the cellulose source material determine the properties of nanocellulose [2]. Acid hydrolysis is by far the widely used method of extraction. During acid hydrolysis, the cellulosic material is exposed to a strong acid at controlled condition namely time, temperature and acid to cellulose source material ratio [1]. Sulphuric acid and other acids such as hydrochloric acid, orthophosphoric acid etc. have been investigated by a number of researchers [2]. However, H_2SO_4 has an advantage of producing stable suspension with high yield of crystallization of CNCs due to sulphate ions [3-5]. This is because the sort of contact between the utilized acid and the cellulose affects the acid hydrolysis reaction. The capacity of cellulose to disseminate and flocculate the aqueous suspension is frequently constrained by HCl. H_2SO_4 tends to interact with the hydroxyl group on the surface of cellulose, producing a charged surface sulphate ester. Consequently, the less thermally stable, more scattered stable suspension [6-8].

Lately, the use of mixture of acids have been investigated with the goal of merging the advantages of acid hydrolysis associated with the use of H_2SO_4 and other acids [9-11]. The resulting CNCs are spherical in shape compared to the rod-like CNCs produced by the single acid. However, the CNCs demonstrates improved thermal properties due to fewer surface sulphate hydroxyl groups. The presence of hydroxyl group at the CNCs surface permits for a number of chemical modifications such as esterification, cationization (etherification), oxidation TEMPO-mediated, polymer grafting, non-covalent and carbamation surface, etc. [2, 12]. The main purpose of chemical modification of CNCs is to improve the properties of CNCs by introducing new properties at the CNC surface [13]. Such properties are dispersions and surface energy compatibility to enhance functionalities of CNCs. Furthermore, it is worth noting that chemical modification of CNCs is only aimed at surface modification [14]. However, it remains a challenge to only alter the surface without altering the CNC morphology [12].

Cellulose esterification is an acetylation chemical modification procedure that uses carboxylic acid agents. During the esterification process, the acylation agents are either exposed to an active derivative (e.g., acid chloride or anhydride) or strong acid catalysis [15]. In a study by Habib et al. (2010) investigated the non-covalent modification of CNCs using phosphoric acid consisting of alkylphenol tails surfactants composed of mono- and di- esters [2]. The modifications resulted in enhanced CNCs dispersions in nonpolar solvents. Moreover, the study showed that using isocratic polypropylene to modify CNCs results in improved compatibility giving extraordinary nucleating agents. In a TEMPO-mediated study using HCl to oxidise the CNC surface resulted in the formation of homogenous suspensions upon dispersion of CNCs in water, while maintaining the CNCs initial morphology [16]. In a Polymer grafting modification study the hydroxyl group is attached onto or from CNCs surface using a coupling agent [17]. The resulting CNCs indicated excellent compatibility and increased adhesion during dispersions in atactic polypropylene solution [2]. It is apparent that all these studies constitute to one common objective, to convey new complex functionalities through modification, and the results are positive [18]. Recently, nucleophilic substitution reactions have been also studied for CNCs modifications where the substitution transpire by means of S_N2 (substitution nucleophilic biomolecular) mechanism at primary carbon positions to decree widespread functionalization [19].

Acetylation of CNCs results in enhanced hydrophobic properties. However, acetylation results in decrease in crystallinity of CNCs. Wu et al. (2018) studied the effect of acetylation of CNCs on the morphology properties [20]. The resulting CNCs displayed the characteristics of the original crystal forms with the rod-like structures remaining intact. Moreover, the acetylation resulted in improved thermal properties. Subsequently, acetylation remains an important modification since it improves CNCs hydrophobicity [20]. Acetylated CNCs incorporated in polymer matrix results in biodegradable nanocomposites (e.g., polylactic acid, PLA) [21]. This demonstrates that acetylated CNCs produces material with greater mechanical properties and superior thermal properties. Such great mechanical properties and ecologically friendly nanocomposites give CNCs a greater depth of application in PLA plastics and reclaimable bioresources utilization [22]. This paper aims at comparing the thermal and morphological properties of green extracted CNCs and the acetylated CNCs.

4.2. Materials and Methods

4.2.1. Materials

Maize Stalk (MS) was collected from the homes of residences at Empangeni (KwaDlangezwa) in KwaZulu natal., South Africa. Sodium hydroxide (NaOH) 99.9%, sodium hypochlorite ($NaClO_2$) 80%, ethanoic acid/ glacial acetic acid (CH_3COOH), sulphuric acid (H_2SO_4) 95-99%, perchloric acid ($HClO_4$) 60%, and toluene (C_7H_8). These chemicals were purchased at Merck chemicals and used without being purified.

4.2.2. Extraction of cellulose

MS was mechanically ground using a Fritsch cutting mill pulveriser 15. Similar method to section 3.2.2 was then followed.

4.2.3. Extraction of cellulose nanocrystals (Green Method)

The dried cellulose was finely grounded using a Fritsch cutting mill Pulveriser 15. A dried mass of 10g of cellulose was weight and transferred to a 600 ml beaker. A volume of 1L deionised water was added to the same beaker. The solution was then stirred using a mechanical stirrer for 24 hours. The cellulose suspension was sonicated for 3 hours in an ultrasonication using ice bath to control the temperature to room temperature. The suspension was then centrifuged for 15 minutes and dried in an oven at 100°C for 24 hours.

4.2.4. Extraction of cellulose nanocrystals

The dry cellulose sample was finely crushed in a Fritsch cutting mill Pulveriser 15. A mass of 15 grams of finely dried cellulose was weighed and transferred into 600 mL beaker. H_2SO_4 at a concentration of 65% was prepared. Similar procedure to 3.2.3 was then followed.

4.2.5. Acetylation of cellulose nanocrystals

A mass of 1g of dried CNCs was weighed and added into a 250 mL beaker. Volumes of 25 mL toluene, 20 mL acetic acid and 0.1 mL perchloric acid were added into the CNCs in a slow sequencing manner while continuously stirring with a PMDC Lab stirrer. After the addition, the solution was further stirred continuously for 1 hour at room temperature. After an hour, the acetylated CNCs (ACNCs) were washed three times with a 1:1 ratio solution of ethanol and distilled water using a centrifuge. The ACNCs were then dried.

4.3. Characterization Methods

4.3.1. Fourier Transform Infra-Red Spectroscopy

Please refer to section 3.3.1.

4.3.2. X-ray Diffraction

Please refer to section 3.3.2.

4.3.3. Scanning Electron Microscopy

Please refer to section 3.3.3.

4.3.4. Thermogravimetric Analysis

Please refer to section 3.3.4.

4.4. Results and Discussion

4.4.1. FTIR spectroscopy analysis

After extracting cellulose using various methods, the FTIR was used to better understand and compare the functional groups associated with green extracted CNCs and the acetylated CNCs. Figure 4.1 depicts the FTIR spectra of raw maize stalk, extracted cellulose, green extracted CNCs, and acetylated CNCs. The natural fiber behaviour of the raw maize stalk was observed with peaks at 3339 cm^{-1} (─OH stretching) due to moisture absorption, 2849 cm^{-1} (C─H vibrations), 1640 cm^{-1} (C=C aromatic vibration), 1368 cm^{-1} (CH_2 bending), 1034 cm^{-1} (C─O stretching), and 893 cm^{-1} [24-29]. The raw maize stalk showed a doublet peak at 2922 cm^{-1} (C─H stretching of methyl group) and 2849 cm^{-1} (C─H stretching of methylene group) which was absent in the extracted cellulose as well as in CNCs due to the removal of methyl group due to the bleaching and alkalization process [30, 31]. In addition, CNCs and extracted cellulose spectra showed a clear addition of a peak at roughly 1310 cm^{-1}, which was absent for

raw maize stalk. The peak could be related to the C─H wagging that occurs when the hydrogen bond is broken [32]. However, removal of the amorphous areas of cellulosic materials resulted in the increase in peak intensity at 892 cm^{-1} [33]. The green extracted CNCs showed a similar peak pattern to the extracted cellulose peak pattern but at lower peak intensity. The acetylation CNCs showed a new absorption peak at around 1255 cm^{-1} assigned to the stretching acetyl C─O groups due to the acetylation process [34]. The intensity of the peaks at 3339 cm^{-1} (─OH stretching) and 1643 cm^{-1} (intramolecular hydrogen bonding) becomes weaker after acetylation due to the acetic anhydride chemical modification [22].

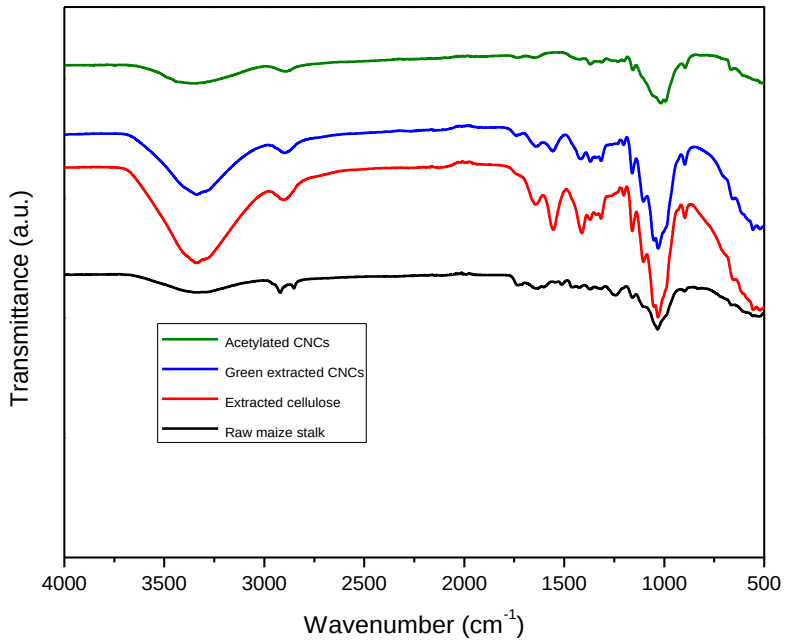

Figure 4.1: FTIR spectra of the raw maize stalk, extracted cellulose, green extracted CNCs, and acetylated CNCs.

4.4.2. X-ray diffraction analysis

XRD was used to investigate and compare the crystallinity of green extracted CNCs and acetylated CNCs. Figure 4.2 shows the XRD spectra of raw maize stalk, extracted cellulose, green extracted CNCs as well as acetylated cellulose. Raw maize stalk, extracted cellulose and green extracted cellulose displayed the main peaks at 2θ = 15.0, 16.4, 22.5 and 35.5°, conforming to the (10), (110), and (200) planes respectively, typical of cellulose I allomorph

[35]. It can be noted that after the acetylation of CNCs, the main peaks at 2θ = 15.0, 16.4, 22.5 and 35.5° were converted to 2θ = 12.0, 20., 21.6 and 35.5° for (10), (110), and (020) planes of cellulose II [36, 37]. This clearly proves that the obtained ACNCs were the allomorph of cellulose II.

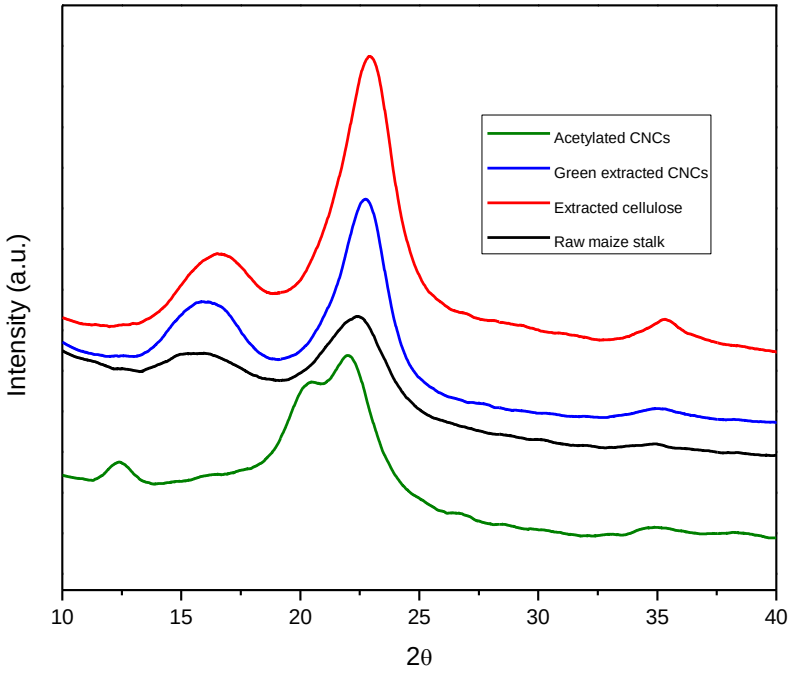

Figure 4.2: XRD spectra of the raw maize stalk, extracted cellulose, green extracted CNCs, and acetylated CNCs.

Table 4.1 shows the crystallinity index values calculated using both the Segal empirical method and the deconvolution method. It can be noted the CI values of raw maize stalk notable increased when compared to all other sample. This feature put further emphasis to the removal of amorphous non-cellulosic material as discussed in FTIR. Where else, the green extracted CNCs displayed a gradual increase in CI compared to the extracted cellulose. This is due to the further removal of amorphous regions. Furthermore, the acetylated CNCs showed the greatest CI values, and this is due to both the acid hydrolysis and the acetylation process which further removed the amorphous regions. The order of crystallinity was observed to be raw maize stalk < extracted cellulose < green extracted CNCs < acetylated CNCs.

Table 4.1. Crystalline Index values of materials studied using Segal and deconvolution methods

Fiber type	**CI (%) (Segal)**	**CI (%) (deconvolution)**
Maize stalk untreated	32	30
Extracted cellulose	80	71
Green extracted CNCs	82	72
Acetylated CNCs	86	74

4.4.3. SEM analysis

SEM was conducted to investigate and compare the morphological properties of green extracted CNCs and the acetylated CNCs. Figure 4.3 shows the SEM images of 4.3(a) raw maize stalk, 4.3(b) extracted cellulose, 4.3(c) green extracted CNCs as well as 4.3(d) acetylated cellulose. It is obvious that there are particles on the surface of the image in Figure 4.3(a). These particles most likely originate from pectin, hemicellulose, and waxes. Additionally, are conspicuously missing from Figure 4.3(b) as a result of the bleaching and alkalization that eliminated these components. Similar observations were made during XRD analysis. In addition, the image showed a rod like shape of CNC fibers with no visible fiber breakages and pull-outs. Figure 4.3(c) showed rod like shaped fibers with characters of deformed shape with no fiber breakage and pull-out observed (see arrows). Figure 4.3(d) showed a completely different shape compared to other materials. The acetylated CNCs showed a structural change from a rod like fiber to a crystal-like structure.

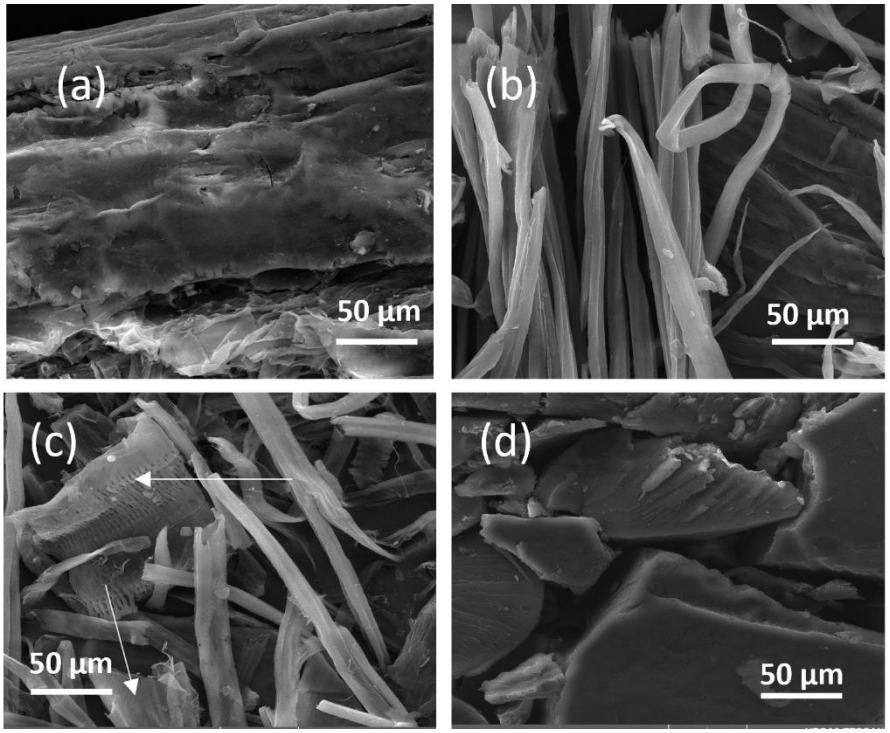

Figure 4.3: SEM images of (a) raw maize stalk, (b) extracted cellulose, (c) green extracted CNCs, and (d) acetylated CNCs.

4.4.4. TGA analysis

Thermogravimetric analysis was used to investigate the thermal properties of the studied materials. TGA and DTG curves of raw maize stalk, extracted cellulose, green extracted CNCs acetylated CNCs are shown in Figure 4.4 and 4.5 respectively. The first weight loss step for all studied material was observed just below 100 °C. This is due to the evaporation of the residual free moisture as displayed by the FTIR absorption peak at around 3339 cm^{-1} [38]. The raw maize stalk displayed two degradation steps at 219 °C and 344 °C. The first degradation step is attributed to the loss of hemicellulose, pectin and waxes while the second degradation step is due to lignin degradation [32, 39-41]. With regards to extracted cellulose, there was a notable increase in thermal stability compared to the raw maize stalk. The increase in thermal stability may be attributed to the removal of amorphous regions during the alkalization and the bleaching steps. The first degradation step was observed at 306 °C while the second at 426 °C due to the removal of lignin.

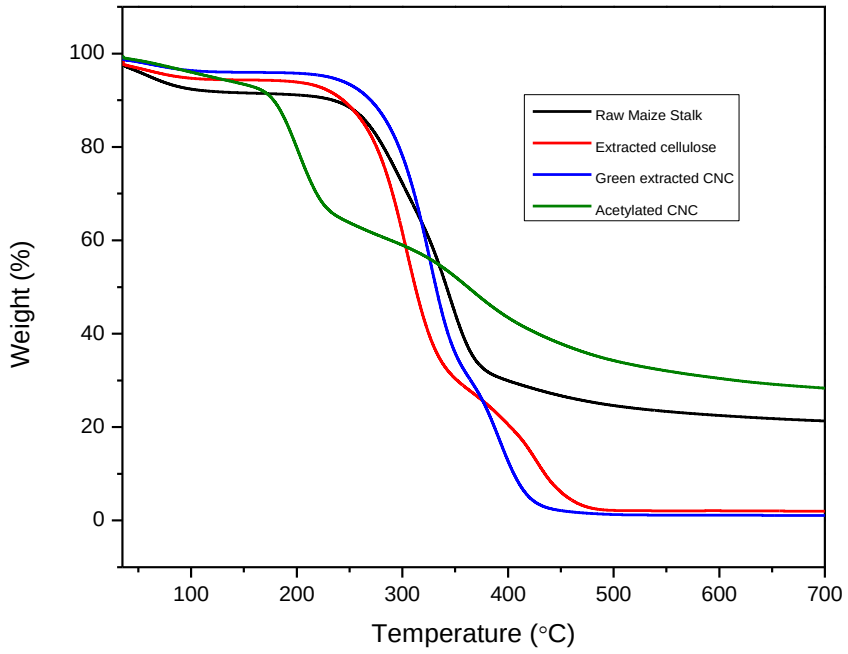

Figure 4.4: FTIR spectra of the raw maize stalk, extracted cellulose, green extracted CNCs, and acetylated CNCs.

In addition, further increase in thermal stability was observed for green extracted CNCs. The first degradation step was observed at 324 °C while the second was observed at 392 °C. Furthermore, the acetylated CNCs displayed two degradation steps at 201 °C and at 361 °C. The thermal stability of ACNCs was observed to be the lowest amongst all the studied material. This may be due to the diversities which are caused by different surface groups which may result in the externally attached polymer and long chain alkane coating. This may result in a new cross-linked material produced from the thermal crosslinking reaction. A relative high char content (30%) was observed for ACNCs. This may be due to the sulphate groups acting as a flame retardant during acid hydrolysis with sulfuric acid [42].

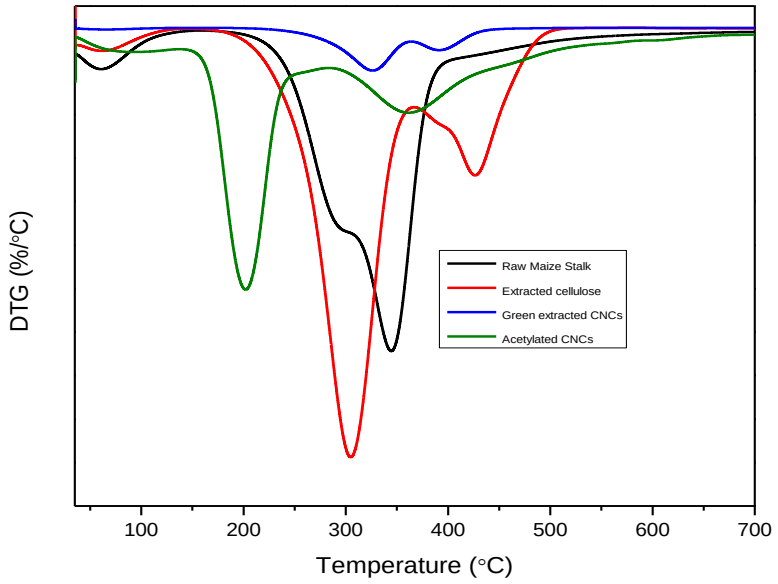

Figure 4.5: DTG spectra of the raw maize stalk, extracted cellulose, green extracted CNCs, and acetylated CNCs.

4.5. Conclusion

The main objective of the study was to investigate and compare the crystallinity, thermal and morphological properties of green extracted CNCs and acetylated CNCs. The acetylated CNCs showed highest crystallinity compared to the green extracted CNCs. The order of crystallinity was observed to be raw maize stalk < extracted cellulose < green extracted CNCs < acetylated CNCs. In addition, there was a transition from cellulose I to cellulose II allomorph upon acetylation of CNCs. In terms of morphology there was a structural transformation upon acetylation of CNC from a rod like fibre to a crystal-like structure. However, acetylation of CNCs produced a less thermal stable material with a higher char content compared to the green extracted CNCs.

4.6. References

1. Arserim-Uçar, D.K., et al., *Characterization of bacterial cellulose nanocrystals: Effect of acid treatments and neutralization.* Food Chemistry, 2021. **336**: p. 127597.
2. Habibi, Y., L.A. Lucia, and O.J. Rojas, *Cellulose nanocrystals: chemistry, self-assembly, and applications.* Chemical reviews, 2010. **110**(6): p. 3479-3500.
3. Pandi, N., S.H. Sonawane, and K.A. Kishore, *Synthesis of cellulose nanocrystals (CNCs) from cotton using ultrasound-assisted acid hydrolysis.* Ultrasonics sonochemistry, 2021. **70**: p. 105353.
4. Ji, H., et al., *Strategy towards one-step preparation of carboxylic cellulose nanocrystals and nanofibrils with high yield, carboxylation and highly stable dispersibility using innocuous citric acid.* Green Chemistry, 2019. **21**(8): p. 1956-1964.
5. Chazeau, L., et al., *Viscoelastic properties of plasticized PVC reinforced with cellulose whiskers.* Journal of Applied Polymer Science, 1999. **71**(11): p. 1797-1808.
6. Yang, X., et al., *Effects of preparation methods on the morphology and properties of nanocellulose (NC) extracted from corn husk.* Industrial Crops and Products, 2017. **109**: p. 241-247.
7. Pan, M., X. Zhou, and M. Chen, *Cellulose nanowhiskers isolation and properties from acid hydrolysis combined with high pressure homogenization.* BioResources, 2013. **8**(1): p. 933-943.
8. Kandhola, G., et al., *Maximizing production of cellulose nanocrystals and nanofibers from pre-extracted loblolly pine kraft pulp: a response surface approach.* Bioresources and Bioprocessing, 2020. **7**(1): p. 1-16.
9. Zhang, H., et al., *Effect of silver contents in cellulose nanocrystal/silver nanohybrids on PHBV crystallization and property improvements.* Carbohydrate polymers, 2017. **173**: p. 7-16.
10. Kassab, Z., et al., *Tomato plant residue as new renewable source for cellulose production: extraction of cellulose nanocrystals with different surface functionalities.* Cellulose, 2020. **27**(8): p. 4287-4303.
11. Corrêa, A., E. de Morais Teixeira, and L. Pessan, *Mattoso LHCJC (2010).* Cellulose nanofibers from curaua fibers. Cellulose. **17**: p. 1183-1192.

12. Eyley, S. and W. Thielemans, *Surface modification of cellulose nanocrystals.* Nanoscale, 2014. **6**(14): p. 7764-7779.
13. Muiruri, J.K., et al., *Highly biodegradable and tough polylactic acid–cellulose nanocrystal composite.* ACS Sustainable Chemistry & Engineering, 2017. **5**(5): p. 3929-3937.
14. Banerjee, M., et al., *Effect of purification methods on commercially available cellulose nanocrystal properties and TEMPO Oxidation.* Processes, 2020. **8**(6): p. 698.
15. Wang, Y., et al., *Functional nanomaterials through esterification of cellulose: a review of chemistry and application.* Cellulose, 2018. **25**(7): p. 3703-3731.
16. Johnson, R.K., A. Zink-Sharp, and W.G. Glasser, *Preparation and characterization of hydrophobic derivatives of TEMPO-oxidized nanocelluloses.* Cellulose, 2011. **18**(6): p. 1599-1609.
17. Habibi, Y., et al., *Bionanocomposites based on poly (ε-caprolactone)-grafted cellulose nanocrystals by ring-opening polymerization.* Journal of Materials Chemistry, 2008. **18**(41): p. 5002-5010.
18. Li, Z., S. Renneckar, and J.R. Barone, *Nanocomposites prepared by in situ enzymatic polymerization of phenol with TEMPO-oxidized nanocellulose.* Cellulose, 2010. **17**(1): p. 57-68.
19. Araki, J., M. Wada, and S. Kuga, *Steric stabilization of a cellulose microcrystal suspension by poly (ethylene glycol) grafting.* Langmuir, 2001. **17**(1): p. 21-27.
20. Wu, Z., et al., *Preparation, characterization and acetylation of cellulose nanocrystal allomorphs.* Cellulose, 2018. **25**(9): p. 4905-4918.
21. Wang, Y., et al., *MDG-1, a polysaccharide from Ophiopogon japonicus, prevents high fat diet-induced obesity and increases energy expenditure in mice.* Carbohydrate polymers, 2014. **114**: p. 183-189.
22. Lin, N., et al., *Surface acetylation of cellulose nanocrystal and its reinforcing function in poly (lactic acid).* Carbohydrate Polymers, 2011. **83**(4): p. 1834-1842.
23. Park, S., et al., *Cellulose crystallinity index: measurement techniques and their impact on interpreting cellulase performance.* Biotechnology for biofuels, 2010. **3**(1): p. 1-10.
24. Kalia, S., et al., *Surface modification of plant fibers using environment friendly methods for their application in polymer composites, textile industry and*

antimicrobial activities: A review. Journal of Environmental Chemical Engineering, 2013. **1**(3): p. 97-112.

25. Wang, L., R. Kumar, and L. Zhang, *Investigation into hemp fiber-and whisker-reinforced soy protein composites.* Frontiers of Chemistry in China, 2009. **4**(3): p. 313-320.
26. Ahmad, E., A. Luyt, and V. Djoković, *Thermal and dynamic mechanical properties of bio-based poly (furfuryl alcohol)/sisal whiskers nanocomposites.* Polymer bulletin, 2013. **70**(4): p. 1265-1276.
27. Hu, F., et al., *Reinforcement and nucleation of acetylated cellulose nanocrystals in foamed polyester composites.* Carbohydrate polymers, 2015. **129**: p. 208-215.
28. Kunaver, M., A. Anžlovar, and E. Žagar, *The fast and effective isolation of nanocellulose from selected cellulosic feedstocks.* Carbohydrate Polymers, 2016. **148**: p. 251-258.
29. Lani, N., et al., *Isolation, characterization, and application of nanocellulose from oil palm empty fruit bunch fiber as nanocomposites.* Journal of Nanomaterials, 2014. **2014**.
30. Motaung, T., et al., *The effect of acid content on the poly (furfuryl) alcohol/cellulose composites.* Polymer composites, 2016. **37**(8): p. 2434-2441.
31. Motaung, T.E., et al., *Agave and sisal fibre-reinforced polyfurfuryl alcohol composites.* Journal of Thermoplastic Composite Materials, 2017. **30**(10): p. 1323-1343.
32. Abidi, N., E. Hequet, and L. Cabrales, *Applications of Fourier transform infrared spectroscopy to study cotton fibers.* Fourier transforms—new analytical approaches and FTIR strategies, 2011: p. 89-114.
33. Pranger, L.A., G.A. Nunnery, and R. Tannenbaum, *Mechanism of the nanoparticle-catalyzed polymerization of furfuryl alcohol and the thermal and mechanical properties of the resulting nanocomposites.* Composites Part B: Engineering, 2012. **43**(3): p. 1139-1146.
34. Liu, L., et al., *Facile preparation PCL/modified nano ZnO organic-inorganic composite and its application in antibacterial materials.* Journal of Polymer Research, 2020. **27**(3): p. 1-11.
35. Xu, J., et al., *Acetylated cellulose nanocrystals with high-crystallinity obtained by one-step reaction from the traditional acetylation of cellulose.* Carbohydrate polymers, 2020. **229**: p. 115553.

36. Jin, E., et al., *On the polymorphic and morphological changes of cellulose nanocrystals (CNC-I) upon mercerization and conversion to CNC-II.* Carbohydrate polymers, 2016. **143**: p. 327-335.
37. Li, X., et al., *Cellulose nanocrystals (CNCs) with different crystalline allomorph for oil in water Pickering emulsions.* Carbohydrate Polymers, 2018. **183**: p. 303-310.
38. Achoundong, C.S., et al., *Silane modification of cellulose acetate dense films as materials for acid gas removal.* Macromolecules, 2013. **46**(14): p. 5584-5594.
39. do Nascimento, D.M., et al., *A comprehensive approach for obtaining cellulose nanocrystal from coconut fiber. Part I: Proposition of technological pathways.* Industrial Crops and Products, 2016. **93**: p. 66-75.
40. Xiong, R., et al., *Comparing microcrystalline with spherical nanocrystalline cellulose from waste cotton fabrics.* Cellulose, 2012. **19**(4): p. 1189-1198.
41. Ianchis, R., et al., *Synthesis and properties of new epoxy-organolayered silicate nanocomposites.* Applied Clay Science, 2015. **103**: p. 28-33.
42. Wu, Q., et al., *The effect of surface modification on chemical and crystalline structure of the cellulose III nanocrystals.* Carbohydrate polymers, 2020. **235**: p. 115962.

CHAPTER 5

EFFECT OF ACID HYDROLYSIS ON PROPERTIES OF CELLULOSE/POLY FURFURAL ALCOHOL (PFA) COMPOSITES FROM MAIZE STALK

(Article Submitted and Accepted for Publication by Wood Research Jour

5.1. Introduction

Lately, the production of biodegradable materials from renewable resources has gained increase interest in preserving fossil resources. Natural fibres such as nanocellulose are interesting bio-based materials for many researchers worldwide due to properties such as low density, low cost and eco-friendliness [1-3]. In fact, nanocellulose has substantial attention in polymer composite materials because of their excellent properties that include non-toxicity and high surface area amongst others [4-10].

CNCs can be extracted by using different methods such as acid hydrolysis, enzymatic hydrolysis and mechanical treatment. However, acid hydrolysis using sulphuric acid remains the widely used method as it requires shorter time and produces stable suspension with high yield and crystallinity. Moreover, it also provides good dispersion as a stable colloid system due to the esterification of hydroxyl group by sulphate ions [11-13]. However, there are several disadvantages associated with the usage of sulphuric acid namely equipment corrosion, low thermal stability of CNCs, large amounts of salt to be disposed amongst others, which limit its usage and applications [14, 15]. Other acids such as hydrochloric acid, acetic acid, maleic acid, nitric acid, phosphoric acid and hydrobromic acid have also been reported in the literature [16-19]. Nonetheless, these acids promote aggregation in most polymers and solvents due to the inter- and intra-molecular hydrogen bonding interaction formed by the abundance of surface hydroxyl groups. Of interest amongst other polymers, is brittleness and biocompatibility of poly furfural alcohol (PFA). Poly furfural alcohol (PFA) is a cross-linked thermosetting polymer produced through a mineral, organic or Lewis acid-catalysed polymerisation of FA. It is comparable to a phenolic resin, but without the toxicity of phenol and formaldehyde compounds. It is used in applications requiring low smoke release, high flame retardancy and char yield. Moreover, it is useful in a number of fields including moulds, corrosion resistant coatings, polymer concrete, metal-casting cores, sand consolidation as well as wood adhesives and binders amongst others [16-19].

There are few studies that have been reported on cellulose/poly furfural alcohol nanocomposite in the literature. Ahmed et. al [3] reported an increased thermal properties and enhanced storage modulus of PFA nanocomposites respectively, as compared to pure PFA. The CNCs used in

the study were prepared via acid hydrolysis using sisal whiskers. Motaung et al. [26] also observed an increased thermal stability and mechanical properties when treated cellulose was blended into PFA matrix. The increase was more pronounced for composites materials predominantly prepared at temperatures above 70 ^{o}C. The similar trend in thermal stability was also observed by Pranger et al. [27]. Moreover, there was a significant increase in the storage modulus of the PFA nanocomposite at low filler content related to the strong reinforcement effect of a well dispersed high-specific surface nanofiller in FA during the sonication step. Similar results in terms of thermal and mechanical properties were also reported in another study [20]. The authors reported an improvement in mechanical and thermal properties when 30% acid hydrolysis was used as compared to 50%. None whatsoever, to the best of our knowledge, investigated effects of hydrolysis by different mixture of acids on the properties of PFA nanocomposites which is the core of the current study. Morphological and thermal properties were studied to better understand the effect of varying acid mixtures during hydrolysis on the properties of cellulose/PFA nanocomposite.

5.2. Materials and Methods

5.2.1. Materials

Maize stalk waste was collected from a local farm around Empangeni, South Africa. $NaClO_2$ (98%), NaOH pellet (99.9%), HCl (32%), H_3PO_4 (85%), H_2SO_4 (98%), HNO_3 (55%), $HClO_4$ (65%) and *p*-toulenesulfonic acid monohydrate were purchased from Laboratory Suppliers, South Africa. Furfural alcohol was obtained from Illovo Sugar (South Africa) Limited Downstream Products Sezela KwaZulu-Natal.

5.2.2. Extraction of cellulose

The maize stalks were mechanically grounded and sieved using a Fritsch cutting mill pulveriser 15. Similar procedure to 3.2.2 was followed.

5.2.3. Extraction of cellulose nanocrystals

The bleached cellulose extracted in 5.2 above was finely crushed in a Fritsch cutting mill pulveriser 15. A finely dry mass of 15 g bleached cellulose was weighed in 5 different 600 ml beakers. The following mixture of acids with concentration of 55% were prepared: H_2SO_4, H_2SO_4/HCl, H_2SO_4/HNO_3, H_2SO_4/H_3PO_4 and H_2SO_4/$HClO_4$. A volume of 250 ml of 55%

H_2SO_4 was added to a beaker in an ice bath of 10°C and stirred with a mechanical stirrer for 30 minutes. Similar procedure to 3.2.3 was then followed.

5.2.4. Preparation of cellulose PFA nanocomposites

A mass of 0.6 g of *p*-toulenesulfonic acid monohydrate was dissolved in 10 ml of distilled water. The prepared catalyst was added dropwise with continuous stirring to 200 ml furfural alcohol (FA). The acid catalysed FA was then slowly added to the cellulose nanocrystals. The mixture was then left at room temperature undisturbed overnight until it solidified. The solidified mixture was then kept at 50°C for 5 days without any disturbance to allow FA to polymerize. This was followed by curing step by further drying the mixture at 100°C for an hour. After an hour, the temperature was further increased to 160°C to achieve the desired degree of polymerization. The composites were then cooled down to room temperature.

5.3. Characterization Methods

5.3.1. Fourier Transform Infrared

Please refer to section 3.3.1.

5.3.2. X-ray Diffraction

Please refer to section 3.3.1.

5.3.3. Scanning Electron Microscopy

Please refer to section 3.3.1.

5.3.4. Thermogravimetric Analysis

Please refer to section 3.3.1.

5.4. Results and Discussion

5.4.1. Fourier transmission infrared

The FTIR spectra of untreated maize stalk, extracted cellulose and various acid hydrolysed CNCs are presented in Figure 5.1. The untreated maize stalk showed characteristic behaviour of natural fibers with peaks observed at 3308 cm^{-1} (─OH stretching), 2902 cm^{-1} (C─H vibrations), 1618 cm^{-1} (C=C aromatic vibration), 1359 cm^{-1} (─CH_2 bending), 1035 cm^{-1} (C─O stretching) and 851 cm^{-1}[1-5,8]. There was a noticeable absence of CH_2 bending and C─O stretching for extracted cellulose, normally attributed to the removal of non-cellulosic materials [26,28]. After acid hydrolysis, all cellulosic characteristic peaks were observed for sulphuric acid and different mixture of acids with an additional peak at 1314 cm^{-1}, attributed to the C─H wagging of hydrogen bond [22]. There was a notable absence of C=O stretching peak at 1737 cm^{-1} for $H_2SO_4/HClO_4$ hydrolysed CNC as compared to other acid hydrolysed cellulose. Like untreated maize stalk, there was a doublet peaks observed at 2902 cm^{-1} (C─H stretching of methyl group) and 2843 cm^{-1} (C─H stretching of methylene group) for H_2SO_4/H_3PO_4 hydrolysed CNC. The doublet peaks can be attributed to H_3PO_4 being a weak acid not strong enough to react with the methylene group of the cellulose.

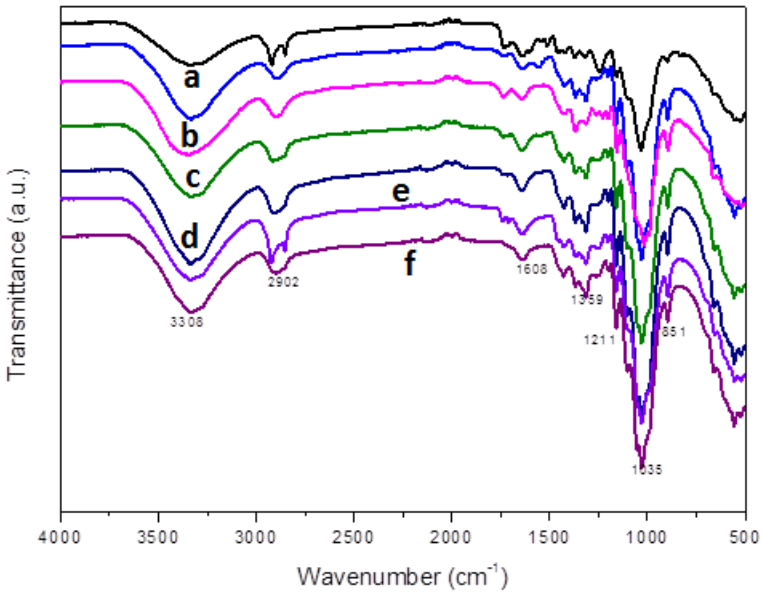

Figure 5.1. FTIR spectra of (a) untreated maize stalk, (b) H_2SO_4 hydrolysed CNC, (c) H_2SO_4/HCl hydrolysed CNC, (d) H_2SO_4/HNO_3 hydrolysed CNC, (e) H_2SO_4/H_3PO_4 hydrolysed CNC and (f) $H_2SO_4/HClO_4$ hydrolysed CNC.

FTIR spectra of pure PFA and various acid hydrolysed CNCs/PFA nanocomposites are shown in Figure 5.2. As usual, the FTIR spectrum of pure PFA displayed main absorption peaks at 2934, 1997 and 1380 cm^{-1} that represent the presence of the aliphatic functional groups [3,26,28]. The stretching vibration of –OH end groups was observed at around 3427 cm^{-1}. Furthermore, there was a noticeable appearance and a gradual increase in the intensity of the new peak at 1267 cm^{-1} for all various PFA nanocomposites. It was also noted that there was diminishing of stretching vibration of the OH- for H_2SO_4/HCl and H_2SO_4/HNO_3 hydrolysed CNCs/PFA nanocomposite. In fact, after encapsulation of various CNCs into the polymer matrix the absorption peaks at 2973 and 2851 cm^{-1} (C-H stretching of methyl and methylene groups respectively) emerged due to the presence of furan rings [26]. Clearly, there were three new peaks at 1420, 1355 cm^{-1} (C-H and C-O bending vibration of hydroxyl respectively) and 855 cm^{-1} (O-H bending vibration of hydroxyl) for all PFA nanocomposites. There was a noticeable similar peaks pattern for H_2SO_4/H_3PO_4 and H_2SO_4 hydrolysed CNCs/PFA nanocomposites. A close look indicated another similarity pattern between H_2SO_4/$HClO_4$ and H_2SO_4/HNO_3 hydrolysed CNCs/PFA nanocomposites. While other researchers attributed the observations to the interfacial interaction [26,28], additionally in this study, the new peaks could be due to the polymerization of FA to PFA which initiates the exfoliation process as it is typically convoyed by a substantial increase of the peak intensity allocated to the skeletal vibration of the 2,5-disubstituated furan rings.

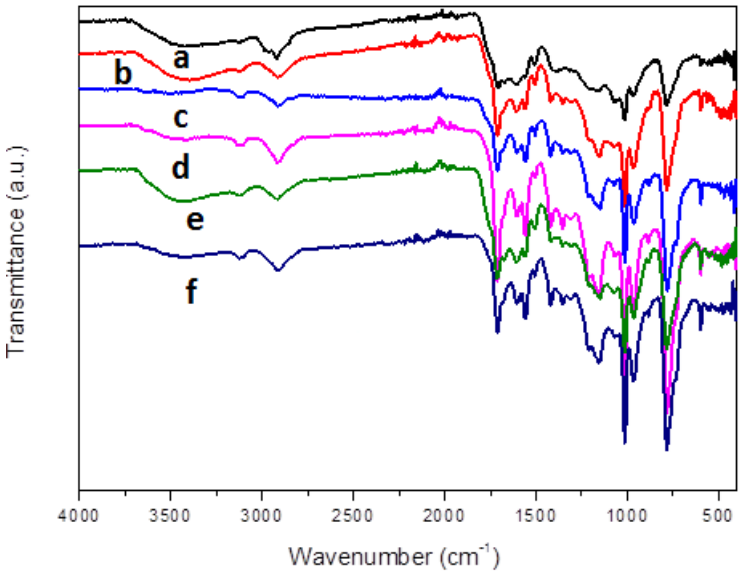

Figure 5.2. FTIR spectra of (a) PFA, (b) H_2SO_4 hydrolysed CNC/PFA, (c) H_2SO_4/HCl hydrolysed CNC/PFA, (d) H_2SO_4/HNO_3 hydrolysed CNC/PFA, (e) H_2SO_4/H_3PO_4 hydrolysed CNC/PFA and (f) H_2SO_4/$HClO_4$ hydrolysed CNC/PFA.

5.4.2. X-*ray* diffraction analysis

XRD spectra of untreated maize stalk, extracted cellulose as well as acid hydrolysed CNCs are shown in Figure 5.3. All samples displayed similar diffraction patterns at 2θ = 15, 23 and 35°, typical of lignocellulosic material [21]. The intensity of the diffraction peak increased after a treatment for all the samples. Of course, that is due to the removal of non-cellulosic materials such as hemicellulose and lignin as confirmed by absence of CH_2 bending and C─O stretching for extracted cellulose from FTIR. Crystallinity index (CI) values calculated using Segal empirical method and deconvolution methods are shown in Table 5.1.

Table 5.1. Crystalline Index values of materials studied using Segal and deconvolution methods

Fiber type	**CI (%) (Segal)**	**CI (%) (deconvolution)**
Maize stalk untreated	32	30
Extracted cellulose	61	63
H_2SO_4 CNC	76	67
H_2SO_4/HCl CNC	83	74
H_2SO_4/HNO_3 CNC	86	77
H_2SO_4/ H_3PO_4 CNC	76	67
H_2SO_4 /$HClO_4$ CNC	61	57

There was a notable increase in CI values for all the samples as compared to untreated maize stalk. That further emphasised the removal of non-cellulosic components as discussed in FTIR. H_2SO_4/HNO_3 is dominant trailed by H_2SO_4/HCl. H_2SO_4/H_3PO_4 hydrolysed CNC and H_2SO_4 hydrolysed CNC appears to have similar CI as confirmed by both Segal and Deconvolution method. In addition, H_2SO_4/$HClO_4$ exhibited the lowest CI compared to the rest. The

observation is attributed to the different strengths of the acid mixtures on the efficiency of non-cellulosic material removal. For instance, both acid blends of the strong HCl and HNO_3 exhibited superior CI values compared to the blend of the weak H_3PO_4.

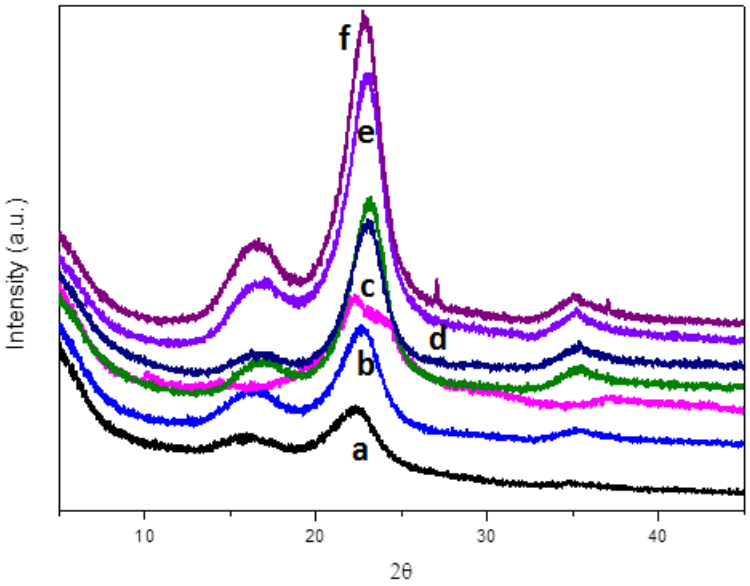

Figure 5.3. XRD spectra of (a) untreated maize stalk, (b) H_2SO_4 hydrolysed CNC, (c) H_2SO_4/HCl hydrolysed CNC, (d) H_2SO_4/HNO_3 hydrolysed CNC, (e) H_2SO_4/H_3PO_4 hydrolysed CNC and (f) $H_2SO_4/HClO_4$ hydrolysed CNC.

XRD patterns of pure PFA and acid hydrolysed CNC/PFA nanocomposites are shown in Figure 5.4. The diffraction pattern of PFA sample showed a single peak at $2\theta = 23°$, which is a similar pattern reported by Lanchis et al. [23]. Similar diffraction pattern was also observed for all nanocomposite, apart from H_2SO_4/H_3PO_4 and H_2SO_4 /$HClO_4$ hydrolysed CNC/PFA nanocomposites respectively. There is no doubt from the literature that peaks for all composites indicated successful compounding of PFA composites [23,28]. The CI values were calculated using the deconvolution method and Segal method as shown in Table 5.1. It was generally clear from the XRD data, that PFA possesses the highest crystallinity than all nanocomposites. The order of crystallinity was reduced with the strength of the acidic medium used. The order of crystallinity was obtained as follows: pure PFA > H_2SO_4 CNC/PFA > H_2SO_4/HCl CNC/PFA > H_2SO_4/HNO_3 CNC/PFA. Both H_2SO_4/ H_3PO_4 CNC/PFA and H_2SO_4 /$HClO_4$ CNC/PFA pattern did not display any peak.

Table 5.2. Crystalline Index values of cellulose (PFA) nanocomposites studied using deconvolution methods.

Fiber type	**CI (%) (deconvolution)**	**CI (%) (Segal)**
PFA	75	61
H_2SO_4 hydrolysed CNC/PFA	67	56
H_2SO_4/HCl hydrolysed CNC/PFA	46	49
H_2SO_4/HNO_3 hydrolysed CNC/PFA	26	32
H_2SO_4/H_3PO_4 hydrolysed CNC/PFA	-	-
H_2SO_4 /$HClO_4$ hydrolysed CNC/PFA	-	-

It is apparent from both methods that the encapsulation of the crystalline CNCs, collapse the resulted crystalline regions in an amorphous cellulose PFA nanocomposites. Taking FTIR results into consideration, it is possible to relate the observation to the emergence of C-H stretching of methyl and methylene groups due to furfural ring interaction with cellulose.

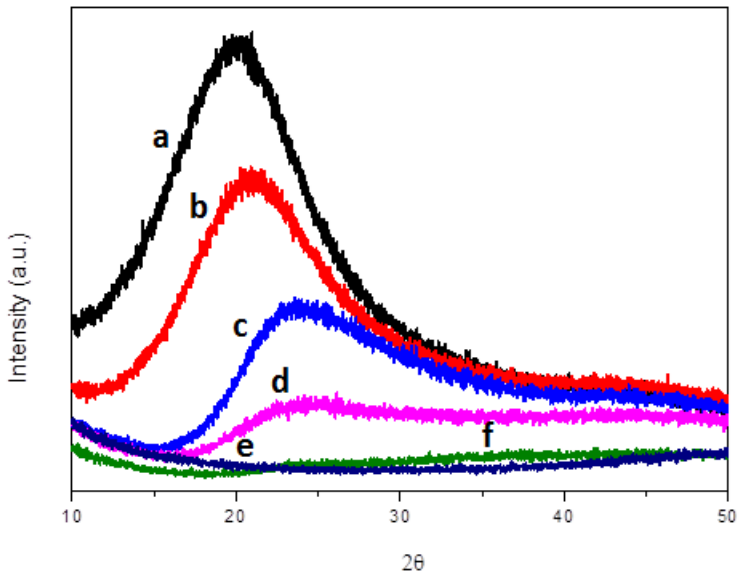

Figure 5.4. XRD spectra of (a) PFA, (b) H_2SO_4 hydrolysed CNC/PFA, (c) H_2SO_4/HCl hydrolysed CNC/PFA, (d) H_2SO_4/HNO_3 hydrolysed CNC/PFA, (e) H_2SO_4/H_3PO_4 hydrolysed CNC/PFA and (f) $H_2SO_4/HClO_4$ hydrolysed CNC/PFA.

5.4.3. Scanning electron microscope

The SEM images of untreated maize stalk, cellulose and acid hydrolysed CNCs are presented in Figure 5.5. Waxes and pectin were clearly noticed on the surface in the form of dispersed particles (Figure 5.5 (a)) which were absent after hydrolysis Figure 5.5 (b). Generally, the treatments reduced fibre size which was initially over 60µm(untreated) to an average of 10µm. It is also worth noting that H_2SO_4 and H_2SO_4/HNO_3 hydrolysed CNC seems to have maintained its rod like structure compared to the rest that appeared a bit deformed (See arrows). In fact, both H_2SO_4/HCl and H_2SO_4/HNO_3 hydrolysed CNCs displayed obvious characters of fibre breakage on the surface. The explanation may not be less than the strength of the acids, as they are considered strong [13,20].

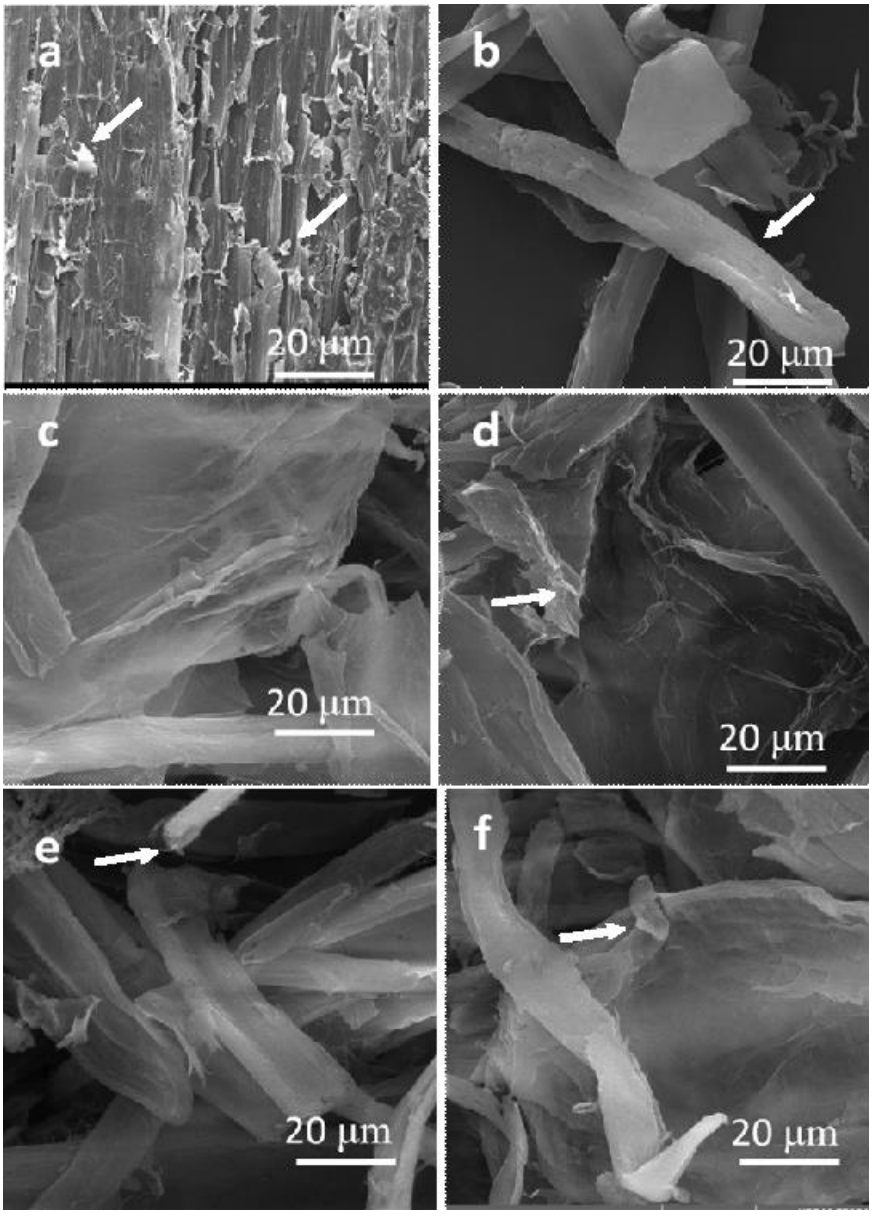

Figure 5.5. SEM images of (a) untreated maize stalk, (b) H_2SO_4 hydrolysed CNC, (c) H_2SO_4/HCl hydrolysed CNC, (d) H_2SO_4/HNO_3 hydrolysed CNC, (e) H_2SO_4/H_3PO_4 hydrolysed CNC and (f) H_2SO_4/$HClO_4$ hydrolysed CNC.

The SEM images of hydrolysed CNC/PFA and various acid mixture hydrolysed CNC/PFA are presented in Figure 5.6. The composites generally showed trapped fibres with others obviously broken and dispersed on the surface. Some, such as **b** and **e**, indicated cavities that are arguably dispersed. This suggests that some of cellulose derivatives, which are (**c, d** and **f**) in this study, generate little or no gas whatsoever during the polymerization of PFA. Despite some cavities

formed in **b**, there is a clear fibre which protruded on the surface, trapped and broken (See arrows). The same observation is also noted at **e**, however in that case most fibres appeared trapped either inside a cavity or adjacent. Furthermore, both **c** and **d** hydrolysed nanocomposites displayed loose fibres embedded in cracks during sample preparation.

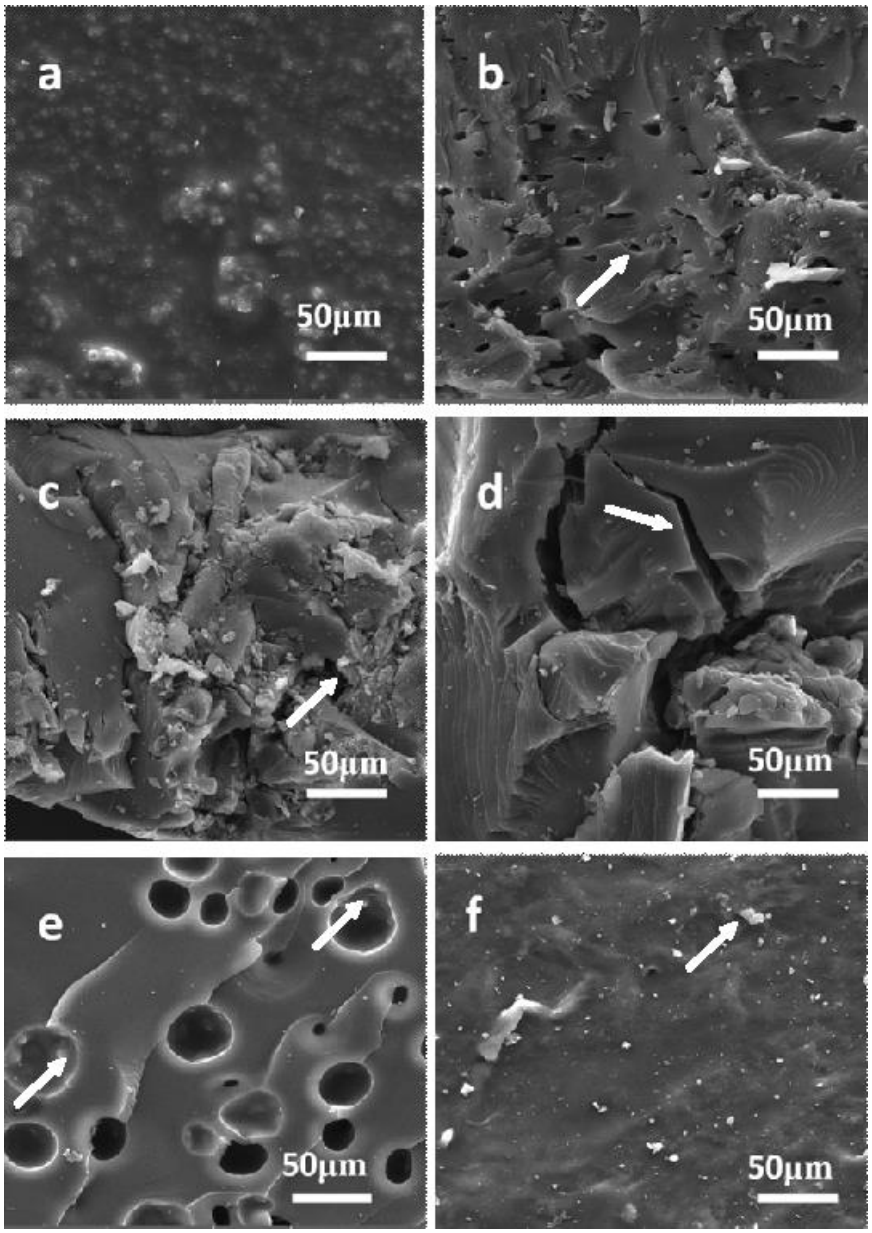

Figure 5.6. SEM images of (a) PFA, (b) H_2SO_4 hydrolysed CNC/PFA, (c) H_2SO_4/HCl hydrolysed CNC/PFA, (d) H_2SO_4/HNO_3 hydrolysed CNC/PFA, (e) H_2SO_4/H_3PO_4 hydrolysed CNC/PFA and (f) H_2SO_4/$HClO_4$ hydrolysed CNC/PFA.

5.4.4. Thermogravimetric analysis

Thermogravimetric analysis studies were conducted to investigate the changes in thermal properties of untreated maize stalk and mixture of acids hydrolysed cellulose. The TGA and DTG curves are shown in Figure 5.7 (A and B). The cellulose spectra display two degradation steps as confirmed by the DTG curve. The first degradation step was attributed to hemicellulose, waxes and pectin while the second step to lignin degradation [24-28]. All the acids hydrolysed CNCs displayed one degradation step between 445 ºC to 460 ºC. There was a notable increase in thermal stability of the acids hydrolysed CNCs compared to untreated maize stalk. The observed increase can be attributed to the further removal of hemicellulose, waxes and pectin from the cellulose during acid hydrolysis, as these components are known to have lower thermal stability compared to pure cellulose [21]. The order of thermal stability was as follows: untreated maize stalk < H_2SO_4 hydrolysed CNC < H_2SO_4/HCl hydrolysed CNC < H_2SO_4/HNO_3 hydrolysed CNC < H_2SO_4/H_3PO_4 hydrolysed CNC <H_2SO_4/$HClO_4$ hydrolysed CNC. Extracted cellulose has lower thermal stability due to lignin and other amorphous regions which degrade at low temperature. The acid strength might be responsible for both H_2SO_4/HCl hydrolysed CNC and H_2SO_4/HNO_3 hydrolysed CNC as they differ by two degrees, the strong acid content could initiate a partial degradation which could result into lower thermal stability. Both H_2SO_4/H_3PO_4 and H_2SO_4/$HClO_4$ hydrolysed CNC showed the highest thermal stability due to the weak acid nature of H_3PO_4 and "moderate" acid nature of $HClO_4$.

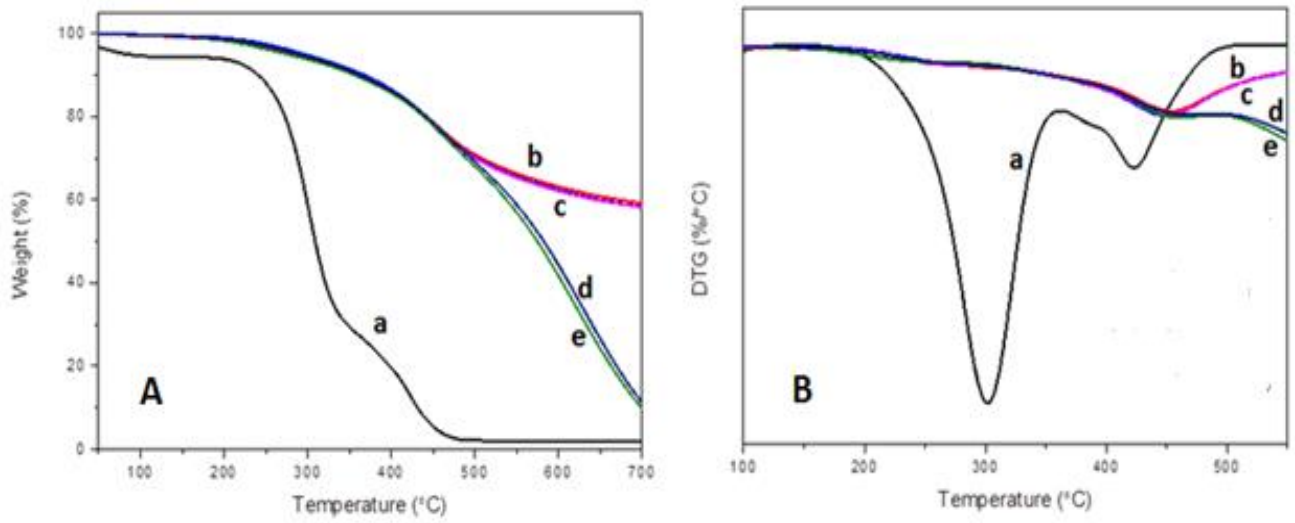

Figure 5.7. TGA(A) and DTG(B) of (a) untreated maize stalk, (b) H_2SO_4 hydrolysed CNC, (c) H_2SO_4/HCl hydrolysed CNC, (d) H_2SO_4/HNO_3 hydrolysed CNC, (e) H_2SO_4/H_3PO_4 hydrolysed CNC and (f) H_2SO_4/$HClO_4$ hydrolysed CNC.

Furthermore, TGA was employed to study the effect of encapsulation of acids hydrolysed CNCs has on the thermal properties of the PFA. The TGA and DTG curves are shown in Figure 5.8 (A and B), respectively. Pure PFA displayed two decomposition steps with the first decomposition step observed around 460 ºC and the second decomposition step around 644 ºC. These degradation steps are due to the removal of oxygen atoms and the alteration of furan rings into a condensed aromatic ring. The H_2SO_4 acid hydrolysed PFA nanocomposite also displayed two degradation steps. The first degradation step was observed around 225 ºC associated to scission of both methyne and methylene links. The second degradation step at high temperature 360 °C was attributed to the scission of furanic links to form ketonic volatile compounds [3]. All the mixture of acids hydrolysed CNCs nanocomposites displayed one degradation step (between 330 and 355 ºC) compared two degradation steps for both pure PFA and H_2SO_4 hydrolysed CNC nanocomposite. It can be noted that H_2SO_4 hydrolysed CNC nanocomposite showed a lower thermal stability than the rest. This could be due to the formation of strong intra- and inter-molecular hydrogen interaction resulted from the aggregation due to the abundance of surface hydroxyl groups. The order of thermal stability was H_2SO_4 hydrolysed nanocomposite < H_2SO_4/HCl hydrolysed nanocomposite < H_2SO_4/HNO_3 hydrolysed nanocomposite < H_2SO_4/$HClO_4$ hydrolysed nanocomposite < H_2SO_4/H_3PO_4 nanocomposite < pure PFA. The order is like the order observed for CNCs and follows the order of acid strength.

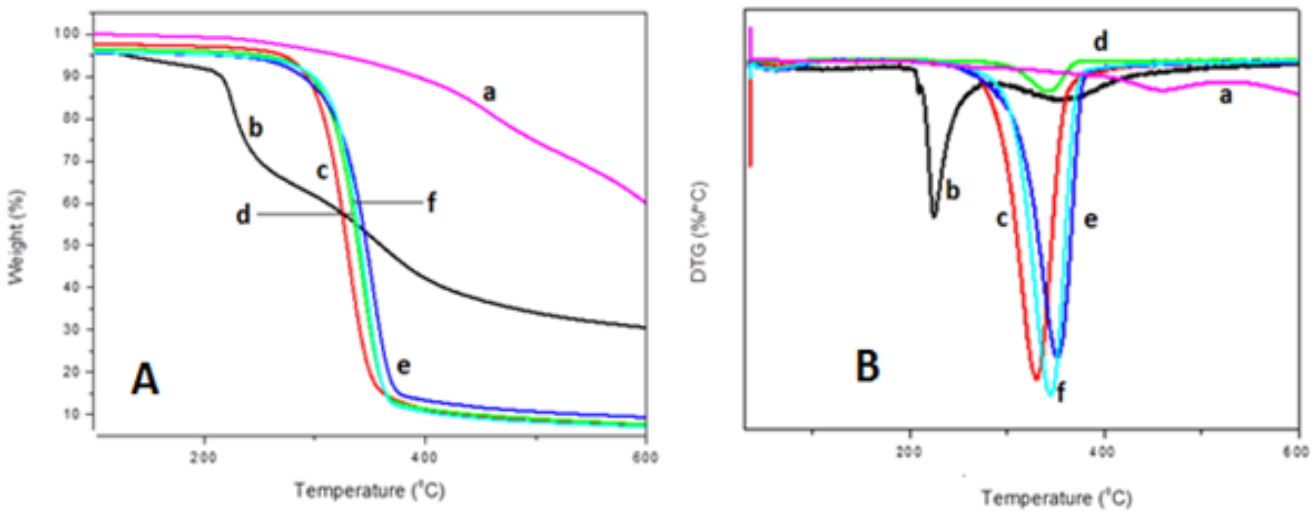

Figure 5.8. TGA(A) and DTG(B) of (a) PFA, (b) H_2SO_4 hydrolysed CNC/PFA, (c) H_2SO_4/HCl hydrolysed CNC/PFA, (d) H_2SO_4/HNO_3 hydrolysed CNC/PFA, (e) H_2SO_4/H_3PO_4 hydrolysed CNC/PFA and (f) H_2SO_4/$HClO_4$ hydrolysed CNC/PFA.

5.5. Conclusion

The main objective of the study was to investigate the effect of acid mixtures on crystallinity, thermal and morphological properties of the resultant CNC/PFA nanocomposites. As expected, there was an increase in crystallinity when extracted cellulose was treated with acid hydrolysis using sulphuric acid as well as mixture of acids. The highest CI were observed for strong acids i.e., H_2SO_4, HNO_3 and HCl. The incorporation of various acids hydrolysed CNC in PFA matrix weakened the crystallinity index of the resultant nanocomposites. It is also known that the usage of sulphuric acid often resultant in low thermal stability of CNCs, which affected the thermal stability of PFA matrix. The H_2SO_4 hydrolysed CNC nanocomposite showed a lower thermal stability than the rest of the nanocomposites. However, there was an improvement with the addition of the second acid with thermal stability depended on the acidic strength. The SEM images echoed both the TGA and crystallinity studies, results with broken trapped fibres and fibre pull-out observed for mixtures using strong acids, i.e., H_2SO_4, HNO_3 and HCl. For mild and moderate acids such as $HClO_4$, the SEM image of H_2SO_4/$HClO_4$ hydrolysed CNC/PFA displayed a fairly good dispersion of CNCs in the PFA matrix with no surface breakage.

5.6. References

1. Kalia, S., et al., *Surface modification of plant fibers using environment friendly methods for their application in polymer composites, textile industry and antimicrobial activities: A review.* Journal of Environmental Chemical Engineering, 2013. **1**(3): p. 97-112.
2. Wang, L., R. Kumar, and L. Zhang, *Investigation into hemp fiber-and whisker-reinforced soy protein composites.* Frontiers of Chemistry in China, 2009. **4**(3): p. 313-320.
3. Ahmad, E., A. Luyt, and V. Djoković, *Thermal and dynamic mechanical properties of bio-based poly (furfuryl alcohol)/sisal whiskers nanocomposites.* Polymer bulletin, 2013. **70**(4): p. 1265-1276.
4. Hu, F., et al., *Reinforcement and nucleation of acetylated cellulose nanocrystals in foamed polyester composites.* Carbohydrate polymers, 2015. **129**: p. 208-215.

5. Kunaver, M., A. Anžlovar, and E. Žagar, *The fast and effective isolation of nanocellulose from selected cellulosic feedstocks.* Carbohydrate polymers, 2016. **148**: p. 251-258.
6. Lefatshe, K., C.M. Muiva, and L.P. Kebaabetswe, *Extraction of nanocellulose and in-situ casting of ZnO/cellulose nanocomposite with enhanced photocatalytic and antibacterial activity.* Carbohydrate polymers, 2017. **164**: p. 301-308.
7. Houdellier, F., et al., *New carbon cone nanotip for use in a highly coherent cold field emission electron microscope.* Carbon, 2012. **50**(5): p. 2037-2044.
8. Lani, N., et al., *Isolation, characterization, and application of nanocellulose from oil palm empty fruit bunch fiber as nanocomposites.* Journal of Nanomaterials, 2014. **2014**.
9. Belloncle, L.C.M.I.C. and B. Cathala, *Extraction and characterization of cellulose nanocrystals from post-consumer wood fiberboard waste.*
10. Candido, R., G. Godoy, and A.R. Goncalves, *Characterization and application of cellulose acetate synthesized from sugarcane bagasse.* Carbohydrate polymers, 2017. **167**: p. 280-289.
11. Yang, X., et al., *Effects of preparation methods on the morphology and properties of nanocellulose (NC) extracted from corn husk.* Industrial Crops and Products, 2017. **109**: p. 241-247.
12. Pan, M., X. Zhou, and M. Chen, *Cellulose nanowhiskers isolation and properties from acid hydrolysis combined with high pressure homogenization.* BioResources, 2013. **8**(1): p. 933-943.
13. Kandhola, G., et al., *Maximizing production of cellulose nanocrystals and nanofibers from pre-extracted loblolly pine kraft pulp: a response surface approach.* Bioresources and Bioprocessing, 2020. **7**(1): p. 1-16.
14. Pandi, N., S.H. Sonawane, and K.A. Kishore, *Synthesis of cellulose nanocrystals (CNCs) from cotton using ultrasound-assisted acid hydrolysis.* Ultrasonics sonochemistry, 2021. **70**: p. 105353.
15. Ji, H., et al., *Strategy towards one-step preparation of carboxylic cellulose nanocrystals and nanofibrils with high yield, carboxylation and highly stable dispersibility using innocuous citric acid.* Green Chemistry, 2019. **21**(8): p. 1956-1964.
16. González, M.M., C. Blanco-Tirado, and M.Y. Combariza, *Nanocellulose as an inhibitor of water-in-crude oil emulsion formation.* Fuel, 2020. **264**: p. 116830.

17. Abd Hamid, S.B., et al., *Synergic effect of tungstophosphoric acid and sonication for rapid synthesis of crystalline nanocellulose.* Carbohydrate polymers, 2016. **138**: p. 349-355.
18. Ghafary, S., et al., *Novel morpholine containing cinnamoyl amides as potent tyrosinase inhibitors.* International journal of biological macromolecules, 2019. **135**: p. 978-985.
19. Souza, A.G.d., et al., *Cellulose nanostructures obtained from waste paper industry: a comparison of acid and mechanical isolation methods.* Materials Research, 2017. **20**: p. 209-214.
20. Motaung, T.E., et al., *Agave and sisal fibre-reinforced polyfurfuryl alcohol composites.* Journal of Thermoplastic Composite Materials, 2017. **30**(10): p. 1323-1343.
21. Park, S., et al., *Cellulose crystallinity index: measurement techniques and their impact on interpreting cellulase performance.* Biotechnology for biofuels, 2010. **3**(1): p. 1-10.
22. Abidi, N., E. Hequet, and L. Cabrales, *Applications of Fourier transform infrared spectroscopy to study cotton fibers.* Fourier transforms—new analytical approaches and FTIR strategies, 2011: p. 89-114.
23. Ianchis, R., et al., *Synthesis and properties of new epoxy-organolayered silicate nanocomposites.* Applied Clay Science, 2015. **103**: p. 28-33.
24. Cruz, G., et al., *Thermal and morphological evaluation of chemically pretreated sugarcane bagasse.* Int. J. Chem. Mol. Nucl. Mater. Metall. Eng, 2013. **7**: p. 435-440.
25. Prins, M.J., K.J. Ptasinski, and F.J. Janssen, *Torrefaction of wood: Part 1. Weight loss kinetics.* Journal of analytical and applied pyrolysis, 2006. **77**(1): p. 28-34.
26. Chen, Z., et al., *Characteristics and kinetic study on pyrolysis of five lignocellulosic biomass via thermogravimetric analysis.* Bioresource technology, 2015. **192**: p. 441-450.
27. Shebani, A., A. Van Reenen, and M. Meincken, *The effect of wood extractives on the thermal stability of different wood species.* Thermochimica Acta, 2008. **471**(1-2): p. 43-50.
28. Mortari, D., M. Britto, and P. Crnkovic, *Correlation between activation energy and thermal decomposition yield of sugar cane bagasse under CO 2/O 2 and N 2/O 2.* Chemical Engineering Transactions, 2014. **37**: p. 31-36.

CHAPTER 6

6.1. Summary and conclusion

The main objective of the study was to investigate the effect of acid mixtures on morphology and thermal properties of CNC/PFA nanocomposites. In addition, the objective was to investigate the effect of $H_2SO_4/HClO_4$ acid mixture concentration on crystallinity, morphology and thermal properties of the resultant CNCs. Furthermore, the other objective was to investigate and compare the crystallinity, morphology and thermal properties of green extracted CNCs and acetylated CNCs. When extracted cellulose was subjected to acid hydrolysis using sulphuric acid as well as a combination of acids, the crystallinity increased as anticipated. The strongest acids, including H_2SO_4, HNO_3, and HCl, had the highest CI. The crystallinity index of the resulting nanocomposites was weakened by the incorporation of various acids that hydrolysed CNC in PFA matrix. It is also well known that using sulphuric acid frequently led to CNCs with low thermal stability, which had an impact on the thermal stability of PFA matrix. Compared to the other nanocomposites, the H_2SO_4 hydrolysed CNC nanocomposite had worse thermal stability. The inclusion of the second acid, whose thermal stability was dependent on its acidic strength, did, however, result in an improvement. The results of the TGA and crystallinity investigations, which showed broken trapped fibers and fiber pull-out for combinations containing strong acids, such as H_2SO_4, HNO_3, and HCl, were confirmed by the SEM images. The SEM picture of $H_2SO_4/HClO_4$ hydrolysed CNC/PFA showed a reasonably good dispersion of CNCs in the PFA matrix with minimal surface breakage for mild and moderate acids like $HClO_4$.

In addition, for the effect of $H_2SO_4/HClO_4$ acid mixture concentration on crystallinity, morphology and thermal properties, the XRD data confirmed an increase in crystallinity following cellulose extraction, with more prominent results following mix acid hydrolysis. The crystallinity index increased when the acid content increased from 45 % to 55 %. Both the SEM and the thermal examinations confirmed the results of the crystallinity tests. For 65 % acid concentrations, the SEM results revealed broken fibers, which caused the crystallinity index readings to decline. The outcomes demonstrated that reduced thermal stability was produced by acid hydrolysis utilizing only H_2SO_4. However, the $HClO_4$ addition increased the thermal stability of CNCs. Lastly, for the comparison of the crystallinity, morphology and thermal properties of green extracted CNCs and acetylated CNCs. When compared to the green extracted CNCs, the acetylated CNCs had the highest crystallinity. Raw maize stalk was found

to have the highest crystallinity, followed by extracted cellulose, green extracted CNCs, and acetylated CNCs. Additionally, the acetylation of CNCs caused a change from the cellulose I to cellulose II allomorph. Upon acetylation, CNC underwent morphological change, going from a rod-like fiber to a crystal-like structure. Contrary to the green extracted CNCs, acetylation of CNCs resulted in a less thermally stable substance with a larger char concentration.

6.2. Recommendation

Based on this study, the following recommendation to further the research into the development of cellulose PFA nanocomposite materials are suggested:

- Because of its extensive agricultural industry, South Africa produces a lot of agricultural waste that is ultimately burned in the atmosphere. For further use in composite materials, further research is therefore required to concentrate on the qualities of this available biomass, such as biodegradability and renewability.
- The thermal and morphological parameters of the mixture of $H_2SO_4/HClO_4$ and H_2SO_4/H_3PO_4 improved. Therefore, additional study is required to enhance the qualities in order to commercialize the material.
- More investigation should be done into the green manufacturing of CNCs since green synthesis is the way of the future for the sustainable development of new materials and for righting the wrongs that humankind has done to the environment.
- The high concentration of hydroxyl groups on cellulose's surface necessitates additional study into functionalising the functional groups for use in packaging, medication delivery, the creation of composite materials, and many other applications.

6.3. Research outputs

- **Stone waste and sustainability** book chapter in "Waste-to-Profit" (W-t-P) *Circular Economy in the Construction Industry for a Sustainable future, Volume 2*, edited by Linda Zikhona Linganiso and Tshwafo Elias Motaung (2019) Chapter 4, New York, Nova Science Publishers.
- Review article: **Preparation and analysis of cellulose PFA composite: critical review.** (Published)
- Research article: **Effect of Acid Hydrolyses on Properties of Cellulose/Poly Furfural Alcohol (PFA) Composites from Maize Stalk.** (Accepted)
- Research article: **The effect of H_2SO_4/$HClO_4$ mixed acid concentration on properties of cellulose nanocrystals from sugarcane bagasse (SCB).** (published)
- Research article: **Morphology and thermal properties comparison of green extracted and acetylated CNCs from maize stalk. (submitted)**